analytica

MDPI

Article

Structural and Functional Properties of a Sulfated Polysaccharide Extracted from Mexican Red Algae

David Encinas-Basurto [1,*], Jorge Márquez-Escalante [1], Karla G. Martínez-Robinson [1], Alma C. Campa-Mada [1], Refugio Pérez-González [2] and Elizabeth Carvajal-Millan [1,*]

[1] Research Center for Food and Development, Carr. Gustavo Enrique Astiazarán Rosas No. 46, Col. La Victoria, Hermosillo 83304, Sonora, Mexico; jorge.marquez@ciad.mx (J.M.-E.); karlagm@ciad.mx (K.G.M.-R.); acampa@ciad.mx (A.C.C.-M.)

[2] Department of Polymer and Materials Research, University of Sonora, Hermosillo 83000, Sonora, Mexico; refugio.perez@unison.mx

* Correspondence: david.encinas@ciad.mx (D.E.-B.); ecarvajal@ciad.mx (E.C.-M.)

Abstract

Sulfated polysaccharides from red algae are multifunctional hydrocolloids whose properties depend strongly on molecular structure, sulfate content, and chain conformation. In this study, a sulfated galactan extracted from *Gracilaria vermiculophylla* collected from a coastal region of northwestern Mexico was investigated to elucidate its structural and functional properties. The polysaccharide was extracted by enzymatic treatment and characterized by monosaccharide analysis, FTIR, 1D/2D NMR spectroscopy, and size-exclusion chromatography coupled with multi-angle light scattering and viscometry. The extracted polysaccharide exhibited high carbohydrate (97%) and sulfate (28%) contents, with galactose as the predominant monosaccharide. It showed a moderate molecular weight (Mw = 2.39 × 10^5 g/mol), a relatively narrow molar mass distribution (Mw/Mn = 1.23), a high intrinsic viscosity (420.9 mL/g), and an Rg/Rh ratio of 2.2, consistent with an expanded macromolecular conformation in solution. The sulfated polysaccharide also exhibited measurable antioxidant activity, particularly in the $ABTS^+$ assay (IC_{50} = 31.8 ± 2.5 mg/mL) compared with the DPPH assay (IC_{50} = 51.1 ± 3.0 mg/mL), and showed Fe^{3+}-responsive association, leading to the formation of microgel-like structures. These findings indicate that the sulfated galactan characterized in this study is a structurally complex and functionally active hydrocolloid with potential relevance for functional food systems and related biomaterial applications.

Keywords: sulfated galactan; red algae; Gracilaria vermiculophylla; hydrocolloids; antioxidant activity

Academic Editors: Dora Melucci and Marcello Locatelli

Received: 31 January 2026
Revised: 16 July 2026
Accepted: 20 July 2026
Published: 23 July 2026

1. Introduction

Marine macroalgae produce unique polysaccharides with diverse properties used in food, medical, and materials science [1]. Sulfated polysaccharides from red algae are notable for their high hydrophilicity, ion responsiveness, and bioactivity, due to sulfate groups along their backbone [2]. These make red algal polysaccharides valuable as food hydrocolloids and functional materials. Their backbone is composed of β-D-galactose and α-L-galactose units, which can be modified to 3,6-anhydrogalactose and, depending on species, substituted with sulfate groups [3]. This structural heterogeneity influences conformation, interactions, gelation, and macroscopic properties such as viscosity, elasticity, and ion sensitivity [4].

Recent studies show that sulfated galactans from red seaweed are responsive macromolecules, not just thickeners, highlighting their versatility and importance in discovering new properties and applications. Hentati, et al. [5] found a sulfated xylogalactan from *Jania adhaerens* has a flexible coil shape (Mw = 8.0 × 10^5 g/mol; [η] = 76 mL/g) and a critical concentration (C* ≈ 7.5 g/L) that exhibits shear-thinning and viscoelasticity, demonstrating that its rheology is sensitive to temperature and ions, indicating that they are tunable biopolymers whose properties depend on more than molecular weight and emphasizing the need for detailed characterization. Recent advances have demonstrated that sulfated polysaccharides (SPs) derived from red marine algae are essential functional components in advanced biomaterial systems. Due to their intrinsic bioactivity and biocompatibility, these compounds enable the development of tunable hydrogels with specific mechanical properties, such as stable and biocompatible scaffolds that promoted calcium deposition by MC3T3-E1 preosteoblasts, highlighting the critical influence of sulfated polysaccharides on viscoelastic behavior and their potential in bone tissue engineering [6].

Importantly, certain sulfated galactans in red algae have an agar-like architecture, enabling them to function as both structurally efficient hydrocolloids and physiologically active macromolecules [7]. This convergence of structure, processability, and functionality confirms sulfated galactans as multifunctional materials, emphasizing the scientific importance of extracting and comprehensively characterizing new polysaccharide sources to better understand structure–property–function relationships. This study aimed to determine the macromolecular characteristics and some functional properties of a sulfated polysaccharide from *Gracilaria vermiculophylla* collected along the northern Pacific coast of Mexico; thereby, new knowledge is described about its diversity and potential applications as a hydrocolloid and functional biopolymer.

2. Materials and Methods

2.1. Materials

Specimens of the red macroalga *Gracilaria vermiculophylla* were manually collected in March 2024 from the intertidal zone of Las Bocas, Sonora, Mexico (26°39′05.7″ N, 109°24′05.5″ W). Taxonomic identification was performed by Dr. Anselmo Miranda-Baeza, a marine biologist from the Laboratory of Marine Aquatic Cultivation Technologies, Universidad Estatal de Sonora, based on the external morphological characteristics of the thalli and comparison with previously identified material from the same region [8–10]. After collection, the samples were rinsed with seawater to remove epiphytes, sand, and debris, transported to the laboratory under refrigerated conditions, dried, and stored until polysaccharide extraction. Deuterium oxide (D_2O, 99.9%) was supplied from Cambridge Isotope Laboratories (Tewksbury, MA, USA), while protease from *Bacillus licheniformis* and other reagents were purchased from Sigma–Aldrich (St. Louis, MO, USA). Ultrapure water (18.2 MΩ·cm) was used for all experimental procedures.

2.2. Extraction and Purification of the Sulfated Polysaccharide

The extraction of the sulfated polysaccharide was carried out according to da Silva Chagas, et al. [11], with minor modifications. Dried algal biomass (5 g) was finely milled and suspended in 500 mL of 0.1 M sodium acetate buffer (pH 5.0) containing EDTA (5 mM) and cysteine (5 mM). The suspension was incubated with protease at 60 °C for 6 h under constant agitation. After enzymatic digestion, the mixture was filtered (1 µm nylon filter discs, Whatman®, Dassel, Germany) to remove insoluble residues, and the polysaccharide was precipitated by adding 16 mL of 10% (*w*/*v*) cetyltrimethylammonium bromide (CTAB). The suspension was kept at room temperature for 24 h and subsequently filtered.

Finally, the precipitate was washed with 0.05% CTAB dissolved in a 2 M NaCl/ethanol solution (100:15, *v*/*v*). The recovered material was dialyzed against distilled water using dialysis tubing with a molecular weight cut-off of 12–14 kDa for 72 h with frequent water changes to remove salts and low-molecular-weight impurities. The dialyzed polysaccharide solution was then reprecipitated by adding absolute ethanol at a solution-to-ethanol ratio of 1:3 (*v*/*v*). The precipitate was recovered by centrifugation and sequentially washed with 80% ethanol, absolute ethanol, and acetone. The final product was dried under a hot-air flow at 60 °C and subsequently lyophilized for further characterization.

2.3. Chemical Composition Analysis

Total carbohydrate content was determined by the phenol–sulfuric acid method, using galactose as the calibration standard [12]. Ash content was measured by incineration of the dried polysaccharide at 550 °C until constant weight. Sulfate content was quantified by the barium chloride–gelatin turbidimetric method after acid hydrolysis, using sodium sulfate as the standard [13]. Extraction yield (%) was calculated based on the dry weight of the initial algal biomass.

2.4. Monosaccharide Composition

The monosaccharide content of the polysaccharides was measured using gas chromatography (GC) on an Agilent HP 6890 GC system (Agilent Technologies, Santa Clara, CA, USA), as described by Rouau and Surget [14]. Polysaccharide samples were hydrolyzed with 3 N H_2SO_4 at 100 °C. The solution was prepared by diluting concentrated sulfuric acid with inositol used as an internal reference. Monosaccharide analysis quantified neutral sugars after acid hydrolysis and conversion to alditol acetates. Sulfated residues and modified sugar units are not fully recovered under these analytical conditions. External calibration was done using glucose, mannose, galactose, xylose, and rhamnose standards (1 mg/mL). Following hydrolysis, monosaccharides were reduced to their corresponding alditols using sodium borohydride and then acetylated with acetic anhydride in the presence of methyl imidazole. The alditol acetates were extracted with chloroform and injected (5 µL) into a DB-225 capillary column (50% cyanopropylphenyl-dimethylpolysiloxane; 30 m × 0.32 mm i.d., 0.15 µm film thickness).

Gas chromatography was performed at 220 °C for the injector with a 1:10 split ratio, 260 °C for the detector, and 205 °C for the oven, with a heating rate of 10 °C/min. Nitrogen was used as the carrier gas, with a constant flow rate of 1.0 mL/min. Flame ionization detectors (FIDs) were employed for detection.

2.5. FTIR Spectroscopy

Fourier-transform infrared (FTIR) spectra of the lyophilized polysaccharide were recorded using an FTIR spectrometer (Is50 Nicolet Thermo Fisher Scientific, Madison, WI, USA) equipped with an ATR accessory. Spectra were collected over 4000–600 cm^{-1} with a resolution of 4 cm^{-1} and averaged over 32 scans. Spectral assignments were made based on characteristic absorption bands reported for sulfated galactans from red macroalgae.

2.6. Nuclear Magnetic Resonance (NMR) Spectroscopy

The structural features of the sulfated polysaccharide were investigated by ^1H and two-dimensional (2D) NMR spectroscopy using a 400 MHz Bruker spectrometer (Bruker BioSpin, Billerica, MA, USA). The sample was dissolved in D_2O (approximately 10 mg/mL) and analyzed at 60 °C to improve spectral resolution.

Two-dimensional experiments, including COSY, HSQC, and HMBC, were performed to obtain proton–proton and proton–carbon correlations. COSY was used to identify scalar couplings within the sugar ring, while HSQC and HMBC provided direct and long-range

^{1}H–^{13}C correlations, respectively. Spectra were processed and analyzed using MestReNova 14.0.0 software (Mestrelab Research, Santiago de Compostela, Spain), and signal assignments were made by comparison with literature data on sulfated galactans from red algae. Due to signal overlap and the structural complexity of sulfated polysaccharides, the assignments should be considered tentative.

2.7. Molecular Weight and Intrinsic Viscosity (SEC–MALS)

Size-exclusion chromatography coupled with multi-angle laser light scattering, viscometry, and refractive index detection (SEC–MALS–VIS–RI) was used to measure the weight-average molar mass (Mw), number-average molar mass (Mn), polydispersity index (I = Mw/Mn), intrinsic viscosity ([η]), radius of gyration (Rg), and hydrodynamic radius (Rh). A DAWN HELEOS-II 8 multi-angle laser light scattering detector, an Optilab T-rEX refractive index detector and a ViscoStar-II viscometer (Wyatt Technology Corp., Santa Barbara, CA, USA) were used for the analyses following previous conditions from our group [15]. SEC–MALS analyses were performed using 50 mM $NaNO_3$ containing 0.02% NaN_3 as the mobile phase (pH ≈ 7.0) at 0.5 mL/min. Polysaccharide samples were dissolved at 5 mg/mL at 80 °C for 1 h to ensure complete solubilization, centrifuged (24,144× *g*, 20 °C, 10 min), and filtered through 0.45 µm membranes prior to injection. Using two Shodex OH-pak columns (SBH-Q-804 and SBH-Q-805, Shodex Showa Denko K.K., Tokyo, Japan), chromatographic separation was performed at a flow rate of 0.5 mL/min using an Agilent HPLC system (G1310B Iso-Pump, G1329B autosampler, G1314F Variable Wavelength Detector; Agilent Technologies, Santa Clara, CA, USA). A refractive index increment (dn/dc) value of 0.146 mL/g, typical for neutral and sulfated polysaccharides in aqueous salt solutions, was used for molar mass determination [16].

2.8. Rheological Measurements

Rheological measurements were carried out using a strain-controlled rheometer (Discovery HR-2, TA Instruments, New Castle, DE, USA) equipped with a 40 mm parallel-plate geometry and a gap of 0.5 mm following reported conditions with some modifications [17]. The sulfated polysaccharide was analyzed at 3% (*w*/*v*). Strain-sweep tests were performed at 25 °C over an oscillatory strain range of 1–25% at a constant frequency of 1 Hz to determine the linear viscoelastic region (LVR). The LVR was defined as the strain range in which G′ remained nearly independent of deformation. Frequency sweep tests were then performed at 25 °C and 2% strain over a frequency range of 0.01–10 Hz. All measurements were performed at least in duplicate, and representative curves are shown.

2.9. Antioxidant Activity of Sulfated Polysaccharides

2.9.1. DPPH Radical Scavenging Activity Assay

The DPPH (2,2-diphenyl-1-picrylhydrazyl) radical-scavenging activity of the sulfated polysaccharide was determined according to Bernal-Mercado, et al. [18] with minor modifications. A 0.1 mM DPPH solution was prepared in ethanol and the absorbance of the $DPPH^{\bullet}$ solution was adjusted to 0.70 measured at 515 nm by proper dilution. A stock solution of the polysaccharide (20 mg/mL) was used. The sample solution was mixed with the DPPH solution at a 1:1 (*v*/*v*) ratio and incubated in the dark at room temperature for 30 min. Absorbance was measured at 517 nm using a GENESYS™ 10UV spectrophotometer (Thermo Scientific, Waltham, MA, USA). All measurements were performed in triplicate. DPPH radical scavenging activity was calculated using the following equation:

$$\text{DPPH scavenging activity } (\%) = \left[1 - \frac{\left(A_{\text{sample},517} - A_{\text{blank},517}\right)}{A_{\text{control},517}}\right] \times 100$$

where $A_{sample,517}$ is the absorbance of the sample, $A_{blank,517}$ is the absorbance of the blank, and $A_{control,517}$ is the absorbance of the control. A calibration curve was constructed using Trolox (11.9–599 µM), and the antioxidant activity of the samples was expressed as µmol Trolox equivalents per gram (µmol TE/g).

2.9.2. $ABTS^+$ Radical Scavenging Activity Assay

The antioxidant activity of the sulfated polysaccharides was evaluated using the $ABTS^+$ (2,2′-azino-bis(3-ethylbenzothiazoline-6-sulphonic acid)) radical scavenging assay, following the method described by Martínez-López, et al. [19]. The radical cation was generated by reacting ABTS with potassium persulfate and was adjusted to an absorbance of 0.70 ± 0.02 at 734 nm using a UV/Vis spectrophotometer (GENESYS™ 10UV, Thermo Scientific, Madison, WI, USA). After combining the polysaccharide sample (20 mg/mL) or Trolox with the $ABTS^+$ reagent, measurements were taken at 30 min time point as reported for polysaccharides previously [20,21]. Trolox (11.9–599 µM) was used to construct the calibration curve under identical experimental conditions. All measurements were performed in triplicate, and the results were expressed in Trolox equivalent.

2.9.3. IC_{50} Determination for Antioxidant Assays

For IC_{50} determination, dose–response curves were constructed for both $ABTS^+$ and DPPH• radical scavenging assays using serial dilutions of the sulfated polysaccharide [22]. The polysaccharide was evaluated over a concentration range of 0.39–100 mg/mL. The $ABTS^+$ and DPPH• radical solutions were prepared as described in Sections 2.9.1 and 2.9.2, respectively.

For each assay, the percentage of radical inhibition was calculated according to the following equation:

$$\% \text{ inhibition} = \frac{A_{control} - A_{sample}}{A_{control}} \times 100$$

where $A_{control}$ is the absorbance of the radical solution without polysaccharide and A_{sample} is the absorbance of the reaction mixture containing the polysaccharide. All measurements were performed in $n = 6$ replicates.

Dose–response curves were generated by plotting percentage inhibition against polysaccharide concentration. IC_{50} values were estimated by linear interpolation between the two concentrations immediately below and above 50% inhibition and expressed as mg/mL. Statistical analysis was performed using SPSS software (version 27, IBM Corp., Armonk, NY, USA). Differences among concentrations were evaluated by one-way analysis of variance (ANOVA), followed by Tukey–Kramer post hoc test. Statistical significance was considered at $p < 0.05$.

2.10. Fe^{3+}-Induced Complexation and Microgel Formation

The interaction between the sulfated polysaccharide and Fe^{3+} ions was evaluated by mixing aqueous polysaccharide solutions (2% w/v) with $FeCl_3$ solutions (0.4% w/v) under gentle stirring, following a previous report from our group [23] with some modifications. Macroscopic changes were visually monitored, and microgel formation was examined by optical microscopy. Microgel-like structure dimensions were estimated from three calibrated optical micrographs using ImageJ software (version 2.9.0, National Institutes of Health, USA). Approximately 20 individual structures were measured per micrograph, resulting in approximately 60 measurements in total. Particle size was expressed as the equivalent circular diameter calculated from the projected area. The measurements were used to provide a descriptive estimate of the apparent size distribution of the Fe^{3+}-induced structures.

3. Results

3.1. Chemical Composition and Extraction Yield

The chemical composition and extraction yield of the sulfated polysaccharide extracted from macroalgae of the species *G. vermiculophylla* are presented in Table 1. The extracted polysaccharide exhibited a very high total carbohydrate content (97.37 ± 0.07%), indicating that the recovered fraction is almost entirely composed of polysaccharide chains. Recent studies on sulfated polysaccharides from *Gracilaria* species report total carbohydrate contents typically ranging from 60% to 90%, depending on species, geographical origin, and purification strategy [24–26]. The exceptionally high carbohydrate content observed in the present study, therefore, suggests efficient removal of non-carbohydrate components, such as proteins, pigments, and low-molecular-weight compounds.

Table 1. Chemical composition and extraction yield of the sulfated polysaccharide.

Composition	Content (%)
Ash	1.4 ± 0.04
Total carbohydrates	97.37 ± 0.07
Sulfate content	28.15 ± 5.30
Yield	27.89 ± 3.70

$\bar{x} \pm s.d$, $n = 4$

The sulfated polysaccharide extraction yield was 27.8 ± 3.7% (dry biomass basis), lying within the upper range of *Gracilaria* species. When aqueous or mild chemical extraction processes are used, a previous study reported yields ranging from roughly 10 to 40%, reflecting the inherent heterogeneity of algal composition and processing techniques. When extraction conditions are set to balance polysaccharide recovery with preservation of sulfate groups and polymer integrity, the yield obtained in this study is comparable to those reported for structurally conserved sulfated polysaccharides. These findings demonstrate that the used extraction procedure enables efficient polysaccharide separation from *Gracilaria* biomass without the need for harsh conditions [27].

All compositional analyses were performed in quadruplicate ($n = 4$), and the low standard deviations obtained for total carbohydrate and ash contents indicate good analytical reproducibility. The relatively larger variation observed for sulfate content is likely associated with the heterogeneous distribution of sulfate ester groups within the polysaccharide population, a characteristic commonly reported for sulfated galactans from red macroalgae [28,29].

The ash content of the sulfated polysaccharide was 1.4 ± 0.04%, which is considered low for polysaccharides derived from marine macroalgae. Recent reports indicate that ash content of *Gracilaria*-derived polysaccharides commonly ranges from 3% to 10%, reflecting their strong association with inorganic salts in seawater [30,31]. Lower ash contents, similar to those observed in the present study, have only been reported when effective desalting and purification protocols were applied [32]. From a physicochemical perspective, minimizing ash content is essential, as residual inorganic ions may screen electrostatic interactions and significantly affect rheological behavior and gelation properties [33].

The sulfate content, expressed as sulfate ions (SO_4^{2-}), was determined to be 28.15 ± 5.3%, indicating that the extracted polysaccharide is highly sulfated. It should be emphasized that total carbohydrate and sulfate contents were determined using independent analytical methods. Therefore, these values are not additive, as sulfate groups constitute substituents attached to the carbohydrate backbone rather than an independent polysaccharide fraction. Recent studies on *Gracilaria* polysaccharides generally report sulfate contents of 5–15% [34], although higher values have been observed, depending

on species, environmental stress, and extraction conditions [35]. The elevated sulfate content observed here suggests a high density of negatively charged groups along the polymer backbone, which is known to promote extended chain conformations, enhance intermolecular repulsion, and favor strong interactions with multivalent cations [2]. Both the degree of sulfation and the location of sulfate along the galactan backbone significantly influence the physicochemical behavior of sulfated polysaccharides from red macroalgae. Gelation behavior and ion responsiveness are strongly impacted by the high density of negative charges introduced by sulfate esters, which alter chain conformation, hydration, and intermolecular interactions [7,24].

Sulfate signals are located in specific local environments that play a part specifically in ion-mediated interactions that promote and facilitate conformational modifications during gelation, according to recent spectroscopic studies [36]. While other sulfation patterns can inhibit chain aggregation and decrease gel stiffness, sulfation at sites like C-6 of galactose has been associated with improved polyelectrolyte behavior and greater sensitivity to multivalent cations [37]. The positional distribution of sulfate groups throughout the polysaccharide backbone is crucial in determining the physicochemical characteristics of sulfated polysaccharides, rather than just the total sulfate content. The addition of sulfate groups at key galactose unit locations (C2, C4, and especially C6) causes noticeable changes in chain structure, molecular weight, and intermolecular interactions, as shown for sulfated arabinogalactans [38]. The relatively higher standard deviation observed for sulfate content (n = 4) may be attributed to the intrinsic heterogeneity of sulfated galactans, which often exhibit non-uniform sulfate distribution along the polymer backbone. Despite this variability, the results consistently indicate a highly sulfated polysaccharide.

Overall, the chemical composition data suggest that the extracted material is a highly purified, strongly sulfated polysaccharide produced at a relatively high yield. These results align with previously reported optimized extraction methods for *Gracilaria* species. The high sulfate content, low inorganic residue, and high carbohydrate purity indicate a polymer system primarily governed by electrostatic interactions and intermolecular associations. These features provide a reliable structural foundation for the rheological properties, physical gel formation, and ion-mediated complexation detailed in later sections.

3.2. Monosaccharide Composition in Sulfated Polysaccharide

The monosaccharide composition of the sulfated polysaccharide extracted from *G. vermiculophylla*, determined by GC–FID after acid hydrolysis, was dominated by galactose (52.03 ± 0.74%), with the presence of arabinose, xylose, mannose, glucose, rhamnose, and fucose as minor components (Table 2). This compositional profile is consistent with sulfated galactans from red macroalgae, which exhibit variable degrees of monosaccharide heterogeneity across species, environmental conditions, and extraction methods [39].

Table 2. Neutral monosaccharide composition of the sulfated polysaccharide determined by GC.

Monosaccharide	Content (%)
Xylose	2.82 ± 0.46
Fucose	0.95 ± 0.34
Rhamnose	0.54 ± 0.19
Arabinose	8.69 ± 2.66
Mannose	2.08 ± 1.28
Galactose	52.03 ± 0.74
Glucose	1.07 ± 0.61

$\overline{x} \pm s.d$, n = 4.

The structure and characteristics of this sulfated polysaccharide are influenced by the prevalence of galactose among the monosaccharides. Instead of rigid, highly ordered structures, these galactose-rich designs promote flexible chain conformations and limit excessive crystalline packing, thereby facilitating the formation of physically crosslinked networks. This galactan structure effectively balances chain organization and electrostatic repulsion upon sulfation, improving network connectivity and responsiveness to ionic environments [28,40]. Consequently, the high galactose content observed in the present sulfated polysaccharide can be regarded as a key structural factor governing its hydration behavior, gel-forming ability, and overall functional performance as a marine polysaccharide. It should be noted that the monosaccharide composition determined by GC-FID represents only the neutral monosaccharides recovered after acid hydrolysis and derivatization. Sulfated sugar residues, 3,6-anhydrogalactose, and partially degraded monosaccharides are not quantitatively recovered under these analytical conditions. Consequently, the summed molar percentages should not be interpreted as representing the total carbohydrate content of the polysaccharide.

A similar galactose-dominated profile was reported for water-extracted sulfated galactans from *Gracilariopsis hommersandii*, where galactose accounted for more than 40–50% of the total monosaccharides, accompanied by variable amounts of 3,6-anhydrogalactose and minor sugars depending on extraction conditions and fractionation strategy [29]. In such systems, galactose-rich backbones provide the structural framework necessary for chain stiffness and extended conformations. At the same time, the presence or absence of cyclized 3,6-anhydrogalactose units and sulfate esters modulates interchain association and gelation behavior. Although the combined compositional analyses strongly support the identification of a highly sulfated galactan, complementary analyses such as ion chromatography or quantitative NMR could provide an independent assessment of sulfate substitution and monosaccharide composition in future studies.

3.3. FTIR of the Sulfated Polysaccharide

The FTIR spectrum of the lyophilized sulfated polysaccharide extracted from *G. vermiculophylla* (Figure 1) shows absorption bands characteristic of sulfated galactans from red macroalgae, allowing the identification of functional groups and providing structural insight into sulfate substitution and backbone features [41,42].

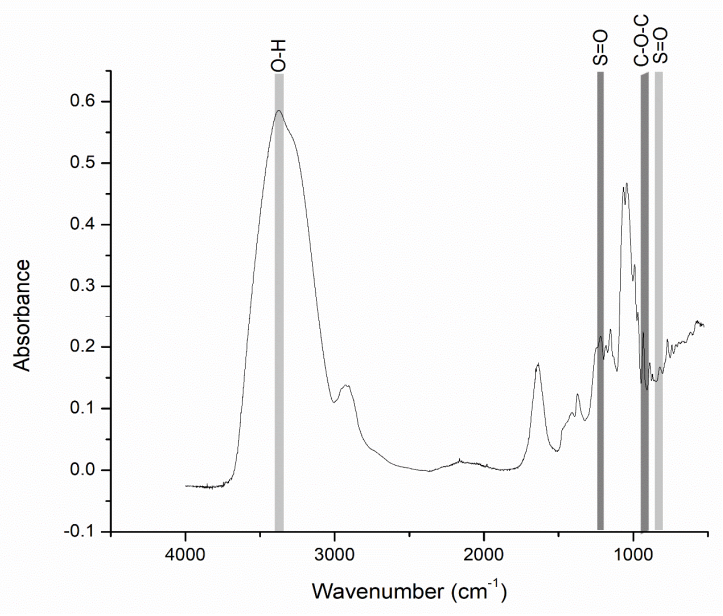

Figure 1. FTIR spectrum of the sulfated polysaccharide extracted from *G. vermiculophylla*.

A broad absorption band centered at 3500–3400 cm^{-1} is attributed to O–H stretching vibrations arising from hydroxyl groups along the polysaccharide backbone and extensive intermolecular hydrogen bonding [43]. This feature is typical of galactan-based polysaccharides and reflects their highly hydrophilic and hydrated nature, as consistently reported for sulfated galactans and agar-derived polymers extracted from red algae [44]. The absorption band observed near 2930–2920 cm^{-1} corresponds to C–H stretching vibrations of aliphatic –CH and $–CH_2$ groups associated with the sugar ring structure (Table 3).

Table 3. FTIR band assignments of the purified sulfated polysaccharide extracted from *G. vermiculophylla*.

Wavenumber (cm^{-1})	Assignment	References
3400–3500	O–H stretching vibrations	[42]
2920–2930	C–H stretching vibrations	[42]
1220–1250	S=O asymmetric stretching	[15,24]
1150–1000	C–O–C/C–O stretching	[45]
930–940	C–O–C vibration of 3,6-anhydrogalactose	[40,42]
815–830	C–O–S vibration	[46]

The asymmetric stretching vibration of sulfate ester groups (S=O) is characterized by a strong, well-defined band between 1220 and 1250 cm^{-1}, supporting the sulfated nature of the polysaccharide. Sulfated galactans from red macroalgae exhibit sulfate ester vibrations in this region, and the intensity of these vibrations has been qualitatively associated with sulfate density [47]. The C–O–C and C–O stretching vibrations linked to glycosidic connections and pyranose ring structures, which make up the fingerprint region of polysaccharides, dominate the spectral region between 1000 and 1150 cm^{-1}. These bands support earlier FTIR research on red algal phycocolloids by confirming a glycosidically connected galactan backbone [15,16].

A distinct absorption band detected at 940–930 cm^{-1} is commonly attributed to vibrations associated with 3,6-anhydrogalactose units, a structural motif frequently reported in red algal galactans [48]. This band has been widely used as a diagnostic marker for galactans containing anhydrogalactose residues. It is typically absent in λ-carrageenans, which lack cyclized 3,6-anhydrogalactose units and lack gel-forming ability. Therefore, the presence of the 930–940 cm^{-1} band supports the non-λ carrageenan of the extracted sulfated galactan and is consistent with the observed physicochemical behavior [41,49].

An absorption band centered in the 830–815 cm^{-1} region was clearly observed. According to established FTIR assignments, this band is generally associated with C–O–S vibrations commonly associated with sulfate substitution involving C-6-related environments of galactose units (galactose-6-sulfate, G6S). Notably, a similar FTIR signature, combining bands near 920–930 cm^{-1} and 820 cm^{-1}, has been reported for funoran, a sulfated galactan from *Gloiopeltis furcata*, where these bands were explicitly correlated with C-6 sulfation and the presence of 3,6-anhydrogalactose units [46,50].

3.4. Nuclear Magnetic Resonance (NMR) Spectroscopy

The structural features of the sulfated polysaccharide extracted from *G. vermiculophylla* were further investigated by ^1H NMR spectroscopy in D_2O at 60 °C. The spectrum exhibited a broad, partially overlapping set of signals in the δ 5.5–3.8 ppm region, characteristic of sulfated galactans from red algae (Figure 2). Notable signals were observed at δ 5.50, 5.30, 5.10, 5.15, 4.6, and 4.8, and a dense region near 4.4–4.5 ppm, indicative of multiple overlapping proton environments within repeating disaccharide units.

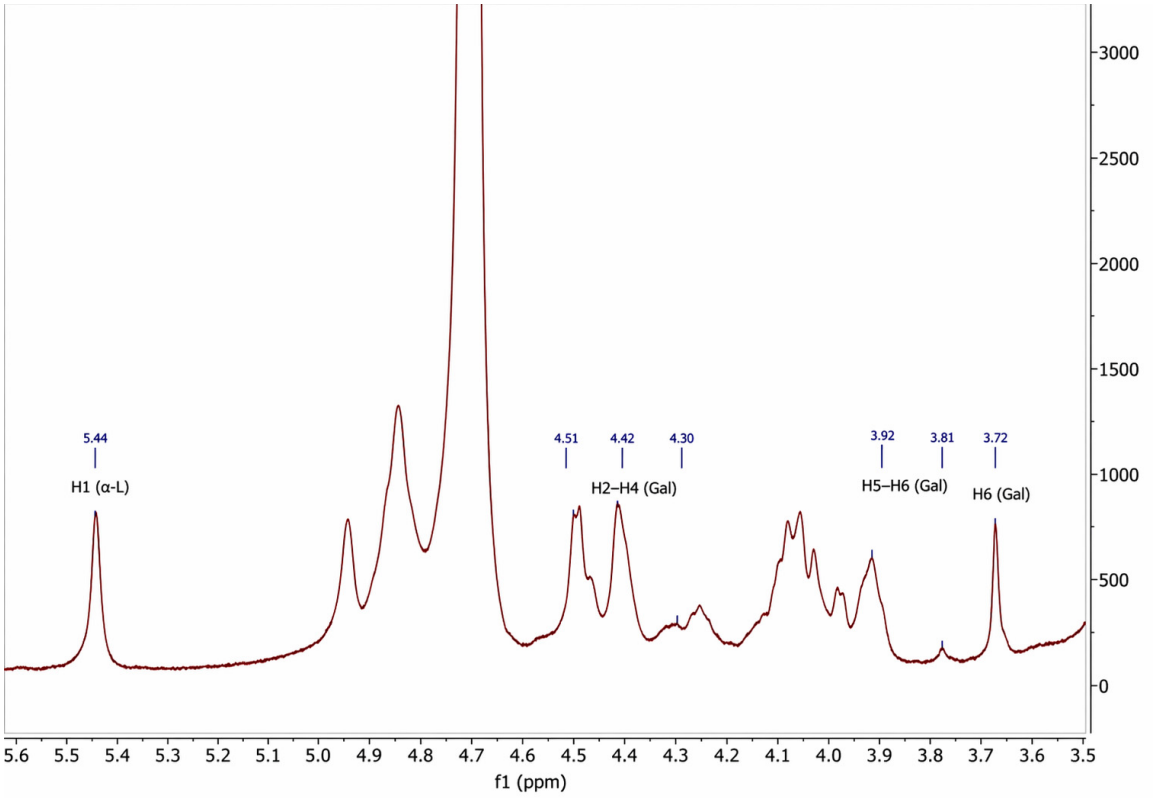

Figure 2. ^{1}H NMR spectrum of the extracted polysaccharide. Signals corresponding to α-L-type anomeric protons (H1), ring protons (H2–H4), and H5–H6 correlations of galactose residues are indicated. Gal: galactopyranosyl residues.

Signals corresponding to both α- and β-galactopyranosyl residues were observed in the anomeric proton region (δ 5.4–4.7 ppm). A signal at δ ~5.4 ppm can be tentatively assigned to α-anomeric protons associated with α-L-galactose derivatives, including 3,6-anhydro-α-L-galactose, a characteristic structural motif of sulfated agarans and related galactans from red algae [28]. Similar chemical shifts have been reported for sulfated agarans extracted from Vertebrata lanosa, where α-L-3,6-anhydrogalactose is a major structural component [48].

Additionally, anomeric signals may be attributed to β-D-galactose-type residues in the δ 4.47 ppm region, consistent with β-(1→3)-linked galactose units forming the backbone of galactan-type polysaccharides. One-dimensional and 2D NMR studies have revealed similar anomeric patterns in sulfated galactans from red algae and marine microalgae, including polysaccharides of the funoran and porphyran types [48,51]. The ring protons (H-2 to H-6) of galactopyranosyl units are located between δ = 4.6 and 3.8 ppm. The extensive signal overlap observed in this region is typical of sulfated polysaccharides, where sulfate ester substitution induces downfield shifts and peak broadening due to strong electronic effects and conformational constraints [52].

Resonances around δ 4.04–4.02 ppm may correspond to H6-related environments influenced by sulfate substitution, glycosidic linkage, or local conformational effects, in agreement with reports of possible C6-related sulfation or sulfate-associated modification in agarans and hybrid funoran/porphyran structures [28]. Overall, the ^{1}H NMR data are consistent with the fact that the extracted polysaccharide is a sulfated galactan mainly composed of galactose units with α- and β-configurations, 3,6-anhydrogalactose residues, and heterogeneous sulfate-associated environments, possibly involving C6-related positions. These structural characteristics support the structural assignments obtained from FTIR

analysis and are in close agreement with recent research on sulfated agarans and hybrid funoran/porphyran polysaccharides from red algae.

The ring protons H2 through H6 of a galactopyranose unit are represented as a cluster of cross-peaks in the 4.3–3.4 ppm proton chemical shift area of the sulfated polysaccharide's 2D COSY spectrum (Figure 3). These cross-peaks are consistent with an intact galactopyranosyl residue and show a continuous network of scalar couplings typical of a galactose spin system. Specifically, the observed successive H2–H3, H3–H4, H4–H5, and H5–H6 cross-correlations are consistent with the expected vicinal coupling topology enclosing the sugar ring [53]. This contiguous spin system is consistent with the connectivity of galactopyranosyl residues within the polysaccharide backbone [50].

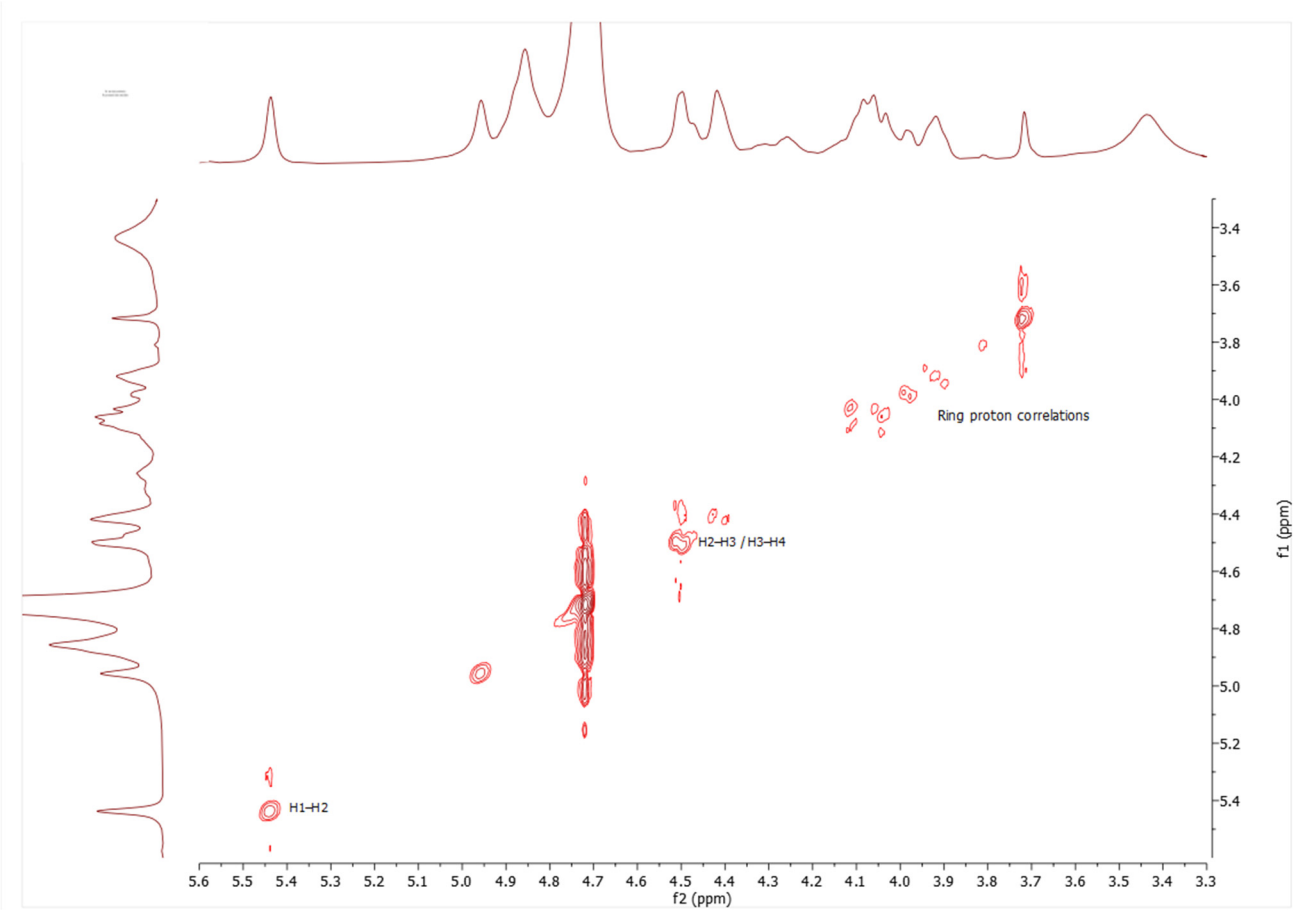

Figure 3. Two-dimensional COSY (^{1}H–^{1}H) NMR spectrum of the sulfated polysaccharide recorded in D_2O.

The COSY spectrum revealed cross-peaks in the δ 3.8–3.5 ppm region, corresponding to H6 protons of galactose residues and their coupling with H5, supporting the presence of H2–H6 connectivity patterns consistent with galactan residues. The chemical shifts observed for H6 are consistent with reported values for red algal sulfated galactans, where H6 protons typically appear in the δ 3.5–4.0 ppm range depending on substitution and local structure [54]. The slight downfield displacement of these signals suggests a modified electronic environment at C6, which has been associated with structural variation such as substitution or conformational effects in agarans and related polysaccharides [11,46,55].

The HSQC spectrum (Figure 4) provided complementary structural information through ^{1}H–^{13}C correlations. A prominent anomeric cross-peak at δH/δC 5.40/99.0 ppm was tentatively assigned to α-L-galactose-derived environments, which may include possi-

ble 3,6-anhydro-α-L-Galp-type units. Additional correlations in the δH 4.45–4.30 ppm/δC 67–70 ppm region were tentatively associated with ring carbons (C2–C5), in agreement with previously reported sulfated galactans exhibiting structural heterogeneity [54]. In the C6 region, two distinct environments were observed. A signal at approximately 60.5 ppm was tentatively assigned to a C6 environment of β-D-galactose-type residues, consistent with a non-substituted primary alcohol. In contrast, a second signal at approximately 69.5 ppm indicated a more deshielded C6-related environment, which may arise from an L-type residue, sulfate substitution, glycosidic linkage, or other local structural effects. Therefore, this signal was interpreted as a modified C6-related environment rather than as definitive evidence of C6 sulfation. This shift is consistent with reported values for agarans, where β-D-galactose C6 typically appears around 60–62 ppm, while L-type or modified residues shift toward ~68–70 ppm [56,57].

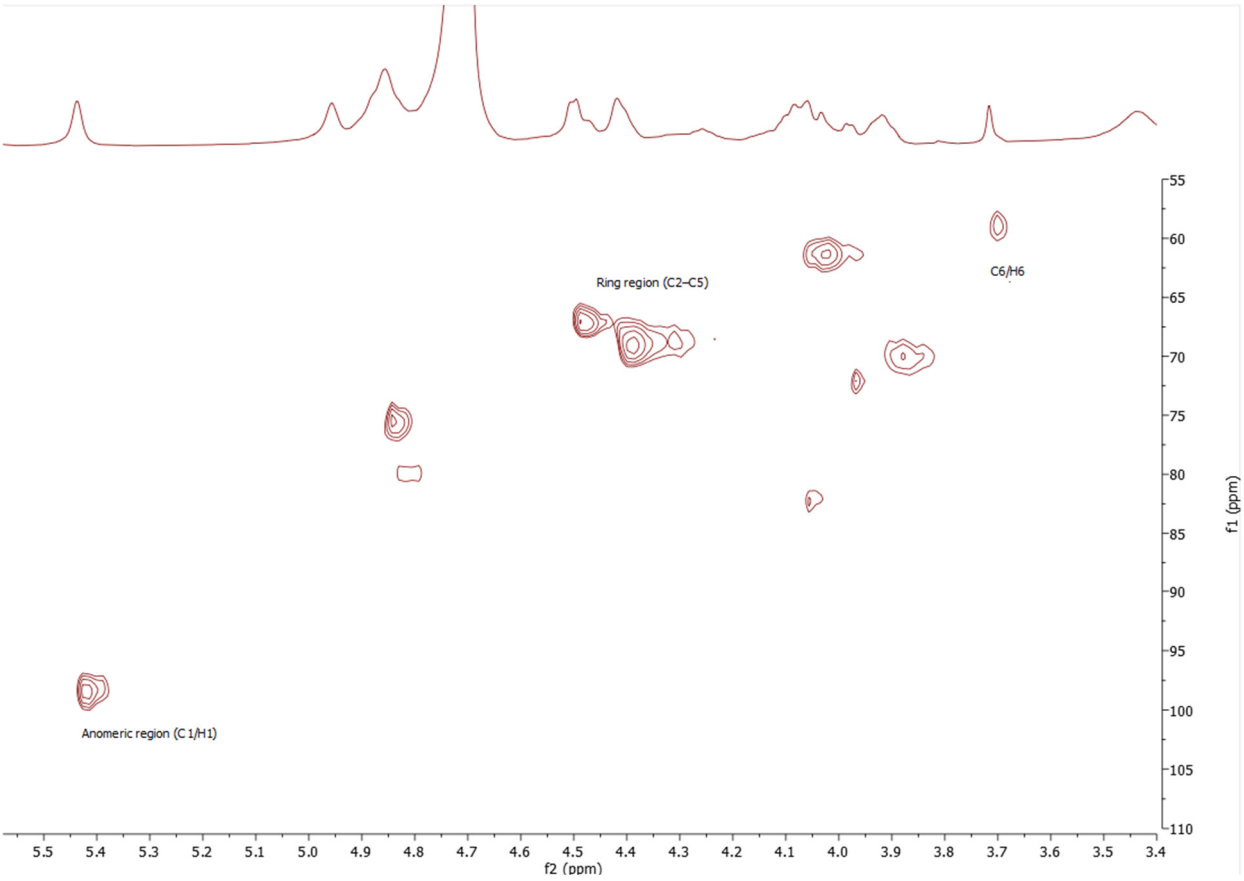

Figure 4. Two-dimensional HSQC (^{1}H–^{13}C) spectrum of the sulfated polysaccharide recorded in D_2O at 60 °C.

The downfield shift of this signal relative to the β-D-galactose C6 correlation observed at δH/δC ~4.00/60.5 ppm indicates a distinct electronic environment, as evidenced by the additional cross-peak at δH/δC ~3.88/69.5 ppm in the HSQC spectrum (Figure 4), consistent with reported values for L-type or structurally modified galactose residues (~69–72 ppm) [58]. This differentiation between two C6 environments is consistent with an agaran-type backbone composed of alternating β-D-galactose and α-L-galactose-derived residues. Similar HSQC patterns, including distinct C6 signals and overlapping ring regions, have been described for sulfated galactans from red algae, reflecting their structural heterogeneity [29].

A previous study from Liu, et al. [56] describes the characterization of sulfated agarose-derived oligosaccharides from *Gracilaria lemaneiformis*, in which agaran-type galactans were fully elucidated using ^{1}H, ^{13}C, and heteronuclear 2D NMR experiments, including HSQC and HMBC [54]. In that study, detailed residue-level assignments suggest alternating β-D-galactose and α-L-galactose units, including 3,6-anhydro-α-L-galactose, and showed that C6-sulfated residues exhibited downfield-shifted H6 signals together with well-defined H5–H6 correlations in COSY spectra. Similarly, Sanchez, et al. [59] reported sulfated galactans displaying anomeric signals in the δ 5.4–4.5 ppm range, along with COSY cross-peaks confirming intact H2–H6 spin systems and H6 chemical shifts influenced by substitution.

In comparison, the present polysaccharide exhibits a similar anomeric distribution (δ 5.5–4.7 ppm), H2–H6 connectivity patterns in COSY, H5–H6 cross-peaks in the δ 3.8–3.5 ppm region, and a characteristic FTIR band at 820–830 cm^{-1}. These features suggest a comparable structural organization consistent with an agaran-type backbone. The HMBC spectrum displayed a correlation at δ 5.45/81.2 ppm, corresponding to a long-range interaction between an anomeric proton and a ring carbon (Figure 5). This correlation is consistent with inter-residue connectivity typically observed in agar-type polysaccharides, supporting possible inter-residue connectivity between galactose-derived units. This finding is consistent with the linkage-related environments within an agaran-type backbone, a fundamental building block of agarose-type polysaccharides previously reported [29,58]. An additional long-range correlation was observed at approximately δH/δC 3.30/68.5 ppm and was tentatively assigned to an H6→C5 correlation within an L-galactose-derived environment. The downfield carbon shift indicates a modified local electronic environment that may be associated with sulfate substitution, glycosidic linkage, or conformational effects. However, because of substantial signal overlap and the absence of an unambiguous residue-specific assignment, this correlation cannot be considered definitive evidence of C6 sulfation. Similar downfield-shifted environments have been reported for sulfated galactans [29,56].

To provide a structural context for the spectral data obtained, the main diagnostic ^{1}H and ^{13}C chemical shift correlations derived from COSY, HSQC, and HMBC experiments are summarized in Table 4. Given the signal overlap characteristic of sulfated polysaccharides, particularly in the ring-proton region (δH 3.8–4.7 ppm), a complete residue-level assignment was not possible. Therefore, the correlations listed should be regarded as tentative diagnostic assignments rather than a complete residue-by-residue structural elucidation.

Table 4. Tentative diagnostic NMR assignments supporting the proposed partial sulfated agaran-type motif.

Residue/Structural Environment	Proton/Correlation	δH (ppm)	δC (ppm)
α-L-Galp-derived/possible 3,6-AnGal-type environment	H-1/C-1	~5.40–5.45	~99–100
α-L-Galp-derived ring region	H-2/H-3	~4.45–4.65	~65–70
α-L-Galp-derived ring region	H-3/H-4	~4.40–4.50	—
β-D-Galp-type environment	H-1/C-1	~4.47	~102
Galactopyranosyl ring region	H-2 to H-5/C-2 to C-5	~3.80–4.70	~67–80
Galactose C6-type environment	H-6/C-6	~4.00	~60.5
Modified C6-related environment	H-6/C-6	~3.88	~69.5
Linkage-related environment	H-1→C-3	~5.45	~81.2
C6-related long-range correlation	H-6→C-5	~3.30	~68.5

Abbreviations: Galp, galactopyranosyl residue; 3,6-AnGal, 3,6-anhydrogalactose residue; α-L and β-D indicate the anomeric configuration and absolute configuration of the sugar residues.

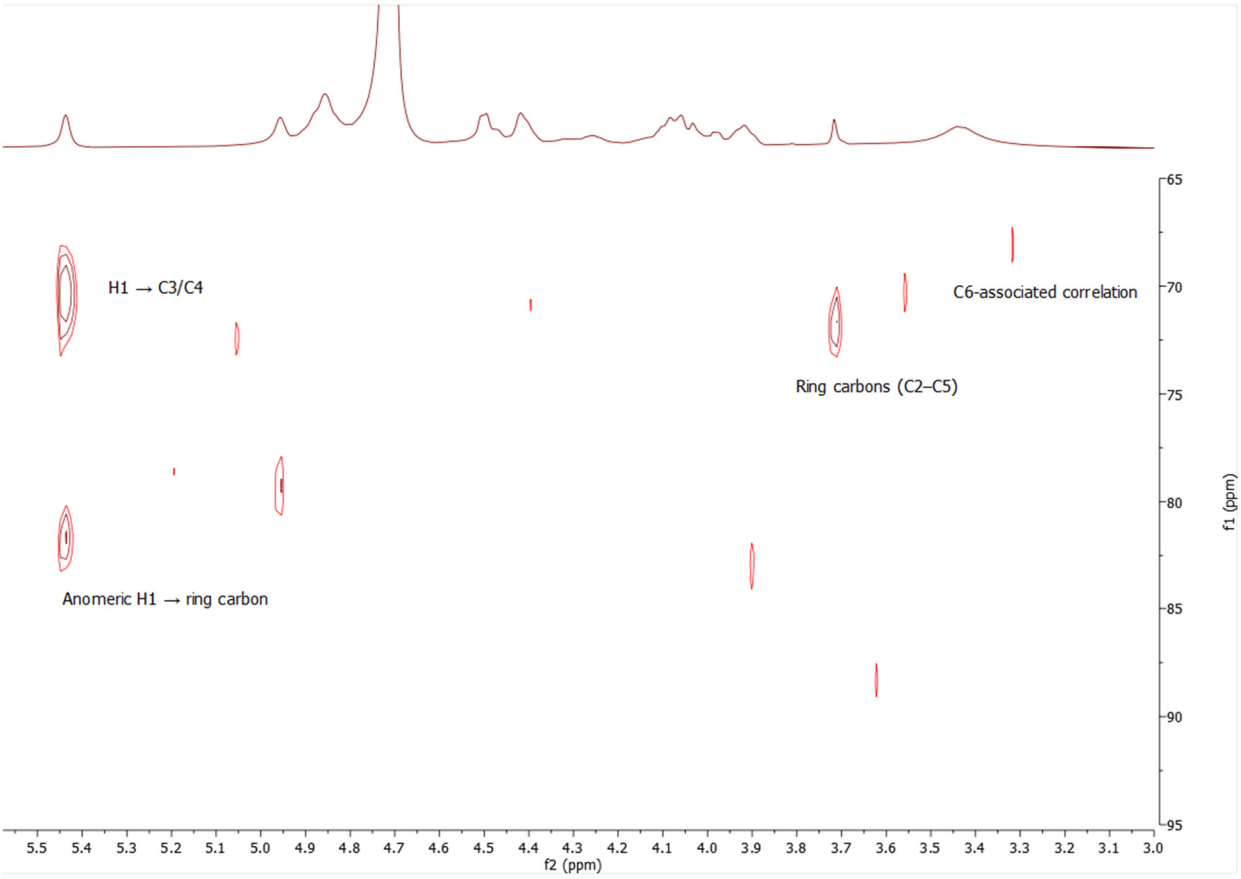

Figure 5. Two-dimensional HMBC (^{1}H–^{13}C) spectrum of the sulfated polysaccharide showing long-range proton–carbon correlations supporting inter-residue connectivity. Spectrum recorded in D_2O at 60 °C.

The NMR data support the presence of β-D-Galp-type and α-L-galactose-derived environments within a sulfated galactan. The α-L-derived residues may include α-L-Galp, α-L-Galp-6S, and possible 3,6-anhydro-α-L-Galp-type units. The possible presence of 3,6-anhydrogalactose-type residues was interpreted from the combined NMR pattern and the FTIR band around 930–931 cm^{-1}. Likewise, the distinct C6-related environments observed by HSQC, together with FTIR bands associated with sulfate ester groups, suggest modified galactose environments possibly associated with C6 substitution or sulfate-related modification. Taken together, the NMR and FTIR data support the presence of a sulfated agaran-type galactan with heterogeneous galactose-derived environments. Nevertheless, the exact sulfate position, residue distribution, and inter-residue connectivity could not be established unambiguously from the available data. In particular, C6 sulfation should be considered a tentative structural possibility rather than a confirmed assignment.

3.5. Molecular Weight and Chain Conformation

Sulfated galactans extracted from red macroalgae are commonly reported to exhibit Mw in the range of 10^5–10^6 g/mol, depending on species, extraction conditions, and purification strategy. The macromolecular parameters of the sulfated polysaccharide obtained in this work, determined by SEC–MALS, are summarized in Table 5. For comparison, an SP from calcareous red seaweed characterized by SEC–MALS was reported to exhibit a Mw of 8.0×10^5 g/mol and a Mn of 1.0×10^5 g/mol, together with a relatively low intrinsic viscosity ([η] = 76 mL/g) and a Rh of 16.8 nm. In contrast, the sulfated polysaccharide analyzed in the present study displays a lower Mw (2.39×10^5 g/mol) but a markedly

higher [η] (420.9 mL/g), indicating a substantially more expanded hydrodynamic conformation. This comparison suggests that differences in backbone composition, sulfation pattern, and chain architecture strongly influence the hydrodynamic behavior of marine sulfated polysaccharides, even when analyzed by the same absolute SEC–MALS methodology. These expanded-chain characteristics are expected to affect chain overlap and network formation under concentrated conditions.

Table 5. Molecular characteristics of the purified sulfated polysaccharide from *G. vermiculophylla* determined by SEC–MALS.

Characteristic	Value
Number-average molar mass (Mn)	1.95×10^5 g/mol
Weight-average molar mass (Mw)	2.39×10^5 g/mol
Polydispersity index (Mw/Mn)	1.23
Hydrodynamic radius (Rh)	23.1 nm
Radius of gyration (Rg)	51.3 nm
Rg/Rh ratio	2.2
Intrinsic viscosity ([η])	420.9 mL/g

These molecular parameters also help explain the weak gel-like behavior observed at 3% w/v. The critical overlap concentration was estimated as C* ≈ 2.4 g/L, while the intrinsic viscosity was [η] = 420.9 mL/g, equivalent to 0.42 L/g. Since the concentration used for gel formation was 3% *w*/*v*, corresponding to approximately 30 g/L, the system was about 12.5 times more concentrated than C*. Similarly, the dimensionless coil-overlap parameter c[η] was approximately 12.6. In polymer solutions, concentrations above C* indicate the transition from isolated polymer chains to a semidilute or concentrated regime, where chain overlap, physical entanglements, and intermolecular associations become increasingly relevant [60]. Therefore, the high c/C* and c[η] values support the formation of a physically associated polysaccharide network, consistent with the weak gel-like behavior observed in the dynamic rheological measurements.

The frequency dependence of tan δ further supported this interpretation. Across the evaluated frequency range, tan δ remained below unity, indicating that the elastic response predominated over the viscous response. However, the frequency-dependent variation in tan δ and the non-negligible viscous contribution suggest a weak physical gel rather than a strong, permanently crosslinked network [61,62].

The SEC–MALS results also provided conformational parameters that help clarify the hydrodynamic behavior of the polysaccharide. The hydrodynamic radius (Rh = 23.1 nm) and radius of gyration (Rg = 51.3 nm) yielded an Rg/Rh ratio of approximately 2.2. The Rg/Rh ratio is commonly used as a conformational descriptor of macromolecules in solution; therefore, the high value obtained here supports an expanded chain conformation rather than a compact globular structure [63]. In sulfated polysaccharides from red algae, SEC–MALS-derived hydrodynamic parameters have been used to distinguish flexible coil-like conformations from more expanded structures [5,26]. Together with the high intrinsic viscosity ([η] = 420.9 mL/g), these results indicate that the sulfated galactan occupies a large hydrodynamic volume, consistent with an expanded, solvated macromolecular structure.

For instance, Khan, et al. [64] reported a weight-average molecular weight (Mw) of 6.15×10^5 g/mol for *Gracilaria blodgettii* polysaccharides. A number-average molecular weight (Mn) of 4.1×10^5 g/mol, together with a polydispersity index (Mw/Mn) of 1.48, indicates a moderately narrow molecular weight distribution. In comparison, the polysaccharide studied in this work has a slightly lower Mw (2.39×10^5 g/mol) but a notably narrower dispersity (Mw/Mn ≈ 1.23), suggesting a higher degree of molecular homogeneity. These comparisons indicate that sulfated galactans can display different degrees of

chain expansion depending on their molecular architecture, sulfate distribution, and extraction history. The SEC–MALS chromatogram (Figure 6) shows a single dominant elution peak with overlapping refractive index (dRI) and light scattering (LS) signals, confirming the presence of a homogeneous macromolecular population and the absence of detectable aggregates or secondary fractions.

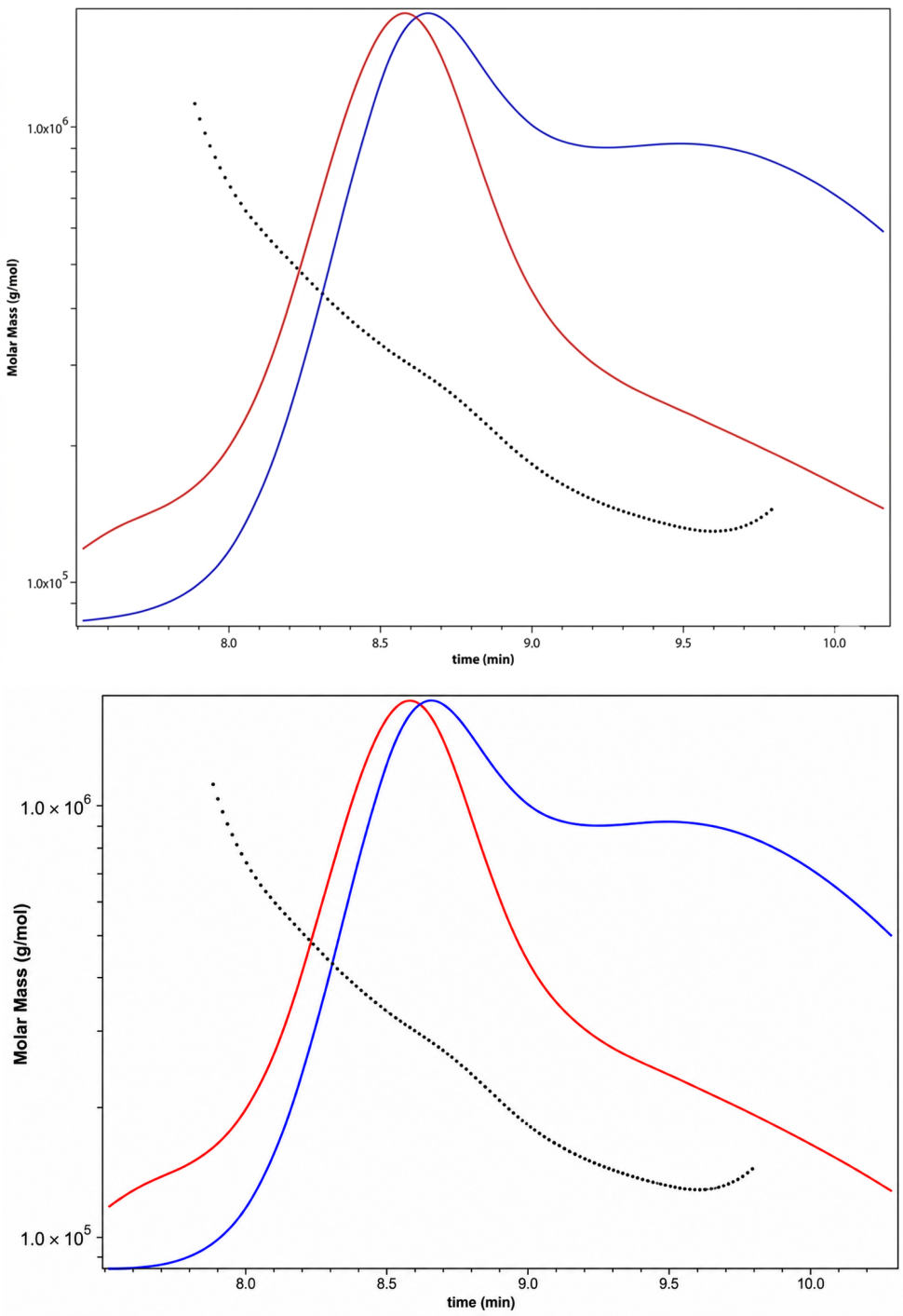

Figure 6. Size-exclusion chromatography coupled with multi-angle light scattering (SEC–MALS) analysis of the sulfated polysaccharide. The differential refractive index (dRI) signal is shown as the blue line, the light scattering (LS) signal as the red line, and the calculated weight-average molecular weight (Mw) along the elution volume as the black line.

By comparison, other sulfated galactans of equal or greater molecular weight exhibit much lower intrinsic viscosities. For instance, a sulfated xylo-galactan from the red seaweed

J. adhaerens [26] with Mw = 6.0 × 10^5 g/mol had [η] = 102 mL/g, and an exopolysaccharide from the microalga *Navicula* sp. with Mw = 1.6 × 10^6 g/mol showed [η] = 197 mL/g [15]. The markedly higher intrinsic viscosity, together with the Rg/Rh ratio of 2.2, supports an expanded hydrodynamic conformation in solution [39]. Such behavior may be associated with the molecular architecture of the sulfated galactan, including backbone composition, sulfate distribution, and the presence of 3,6-anhydrogalactose-type residues. Notably, the measurement was carried out in 50 mM $NaNO_3$, which reduces polyelectrolyte effects [60], so the high [η] is attributable to the polymer's innate chain architecture rather than charge-induced expansion [65].

In practical terms, the high intrinsic viscosity ([η] = 420.9 mL/g) indicates a large hydrodynamic volume of the polymer chains in solution [66]. Using the classical approximation $c^* = 1/[\eta]$, the critical overlap concentration is estimated to be approximately 2.4 g/L. This low c^* value suggests that chain interpenetration and physical entanglements occur at very low polymer concentrations, providing a structural basis for the pronounced viscosity increase and the formation of physically crosslinked networks observed even in the absence of added ions [67].

The macromolecular characteristics described above, particularly the high intrinsic viscosity and relatively expanded chain conformation, suggest that the sulfated polysaccharide is capable of forming intermolecular associations in aqueous solution. At concentrations above the overlap concentration (C*), such interactions are expected to promote chain entanglement and the formation of transient network structures [68]. In this context, rheological analysis provides a direct approach to evaluate how these molecular features translate into macroscopic viscoelastic behavior. Therefore, strain and frequency sweep experiments were performed to characterize the mechanical response and structural stability of the polysaccharide network.

To ensure that oscillatory measurements were conducted within the linear viscoelastic region (LVR), strain sweep experiments were performed at constant frequency (1 Hz) over a deformation range of 1–30% (Figure 7). The storage modulus (G′) remained nearly constant up to approximately 5% strain, indicating that the system behaves linearly within this region. Beyond this point, a progressive decrease in G′ and a concomitant increase in G″ were observed, suggesting structural disruption of the polymer network.

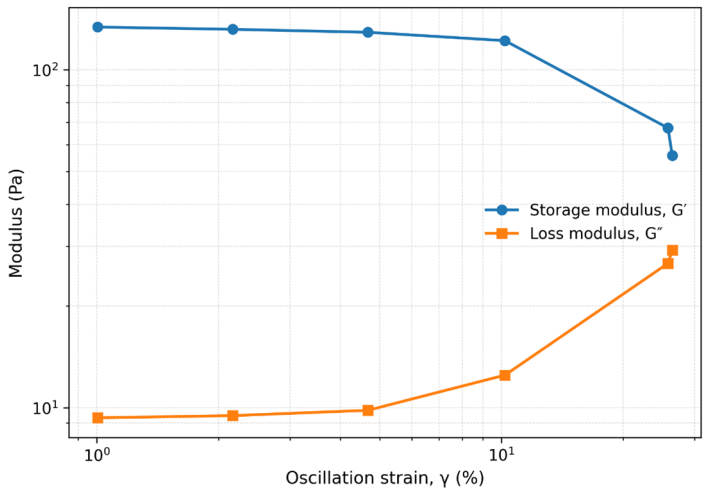

Figure 7. Strain sweep of the sulfated polysaccharide hydrogel (3% *w*/*v*) at 25 °C and 1 Hz, showing the storage modulus (G′) and loss modulus (G″) as a function of oscillatory strain. The linear viscoelastic region (LVR) is observed up to approximately 5% strain.

The presence of a defined LVR and relatively stable G′ values within this region suggests the formation of a weakly structured network, typical of physically entangled, weakly crosslinked polysaccharide systems. This behavior is likely governed by a combination of intermolecular hydrogen bonding, chain entanglement, and electrostatic interactions arising from the high sulfate content of the polymer. In sulfated galactans, the presence of charged groups promotes extended chain conformations and modulates intermolecular interactions, directly influencing viscoelastic properties and network stability [2,28]. Similar weak gel behavior, characterized by G′ > G″ and moderate frequency dependence, has been widely reported for marine polysaccharides, where the balance between chain flexibility, charge density, and intermolecular interactions determines the mechanical response of the system [55,69].

Based on these results, a strain value of 2% was selected for frequency sweep measurements, as it lies well within the LVR and ensures that the viscoelastic response reflects the intrinsic network structure rather than strain-induced artifacts. Frequency-sweep experiment revealed that G′ remained higher than G″ across the entire frequency range (Figure 8), confirming the predominance of elastic over viscous behavior. The G′ values were on the order of 10^1–10^2 Pa, while G″ remained lower, typically within the 10^1 Pa range. Both moduli exhibited moderate frequency dependence, characteristic of weak gel systems, with G′ showing higher absolute values and slightly stronger dependence than G″. This behavior is indicative of a structured network stabilized by physical interactions, such as ionic crosslinking and hydrogen bonding [55].

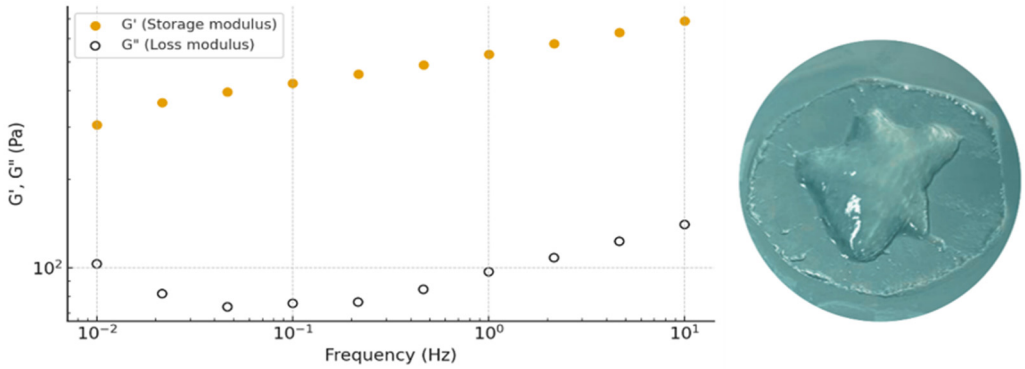

Figure 8. Frequency dependence of the storage modulus (G′) and loss modulus (G″) of the sulfated polysaccharide hydrogel (3% *w*/*v*) measured at 25 °C and 2% strain within the linear viscoelastic region.

The frequency dependence of tan δ was also evaluated to describe further the viscoelastic balance of the 3% *w*/*v* polysaccharide dispersion (Figure 9). Across the evaluated frequency range, tan δ remained below unity, indicating that the elastic response predominated over the viscous response. However, the frequency-dependent variation in tan δ and the non-negligible viscous contribution suggest a weak physical gel rather than a strong, permanently crosslinked network. *G. vermiculophylla* produces agar with structural variations depending on the species and extraction conditions. Li, et al. [45] studied polysaccharides from *Gracilaria chouae* collected from five different regions, and all samples exhibited weak gel behavior at 1% *w*/*v* and 25 °C. At low frequencies, some samples exhibited a predominance of the elastic modulus over the viscous modulus, indicative of a more solid-like response, whereas others showed dominant viscous behavior; however, as the frequency increased, all samples converged toward tan δ values close to 1, supporting their classification as weak gels [69].

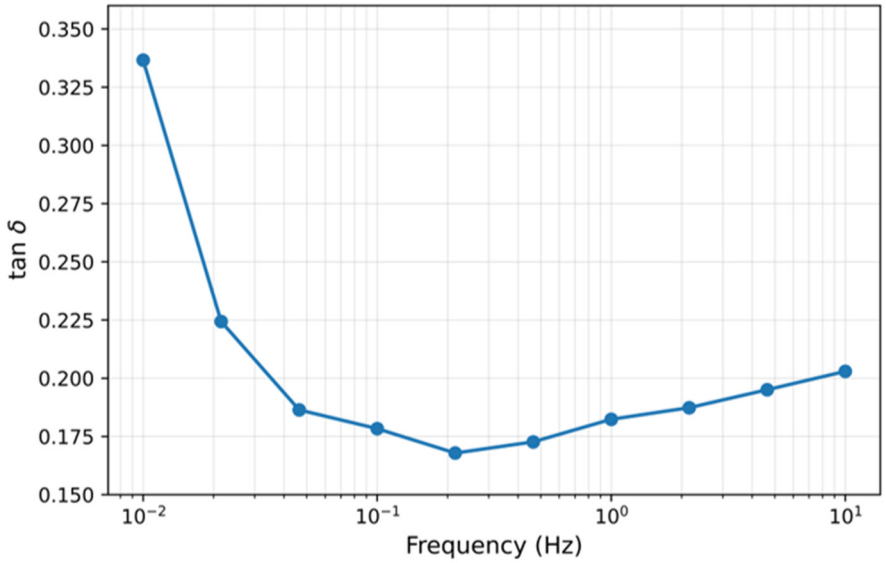

Figure 9. Frequency dependence of tan δ for the 3% *w*/*v* sulfated polysaccharide dispersion.

The predominance of the elastic modulus over the viscous modulus (G′ > G″) at low frequencies is commonly interpreted as solid-like or gel-like behavior, indicating the formation of a weak yet structured polysaccharide network. In general, higher 3,6-anhydro-L-galactose content and lower sulfation result in stronger gels (high G′), while sulfates in certain positions prevent double helix formation, weakening the gel or preventing its formation [70,71].

3.6. Antioxidant Activity of Macroalgae Sulfated Polysaccharide

The antioxidant activity of the sulfated polysaccharide extracted from red marine algae was clearly evaluated by both $ABTS^+$ and DPPH radical scavenging assays. The significantly higher value obtained in the $ABTS^+$ assay (172.4 ± 6.8 µmol TE/g) compared to the DPPH• assay (51.1 ± 3.0 µmol TE/g, expressed as Trolox equivalents) suggests greater reactivity in aqueous/polar radical systems, which is typical of highly charged and hydrophilic polysaccharides with abundant sulfate ester groups.

The antioxidant capacity values obtained in the $ABTS^+$ and DPPH• assays fall within the range reported for purified sulfated polysaccharides from marine sources, which generally exhibit moderate antioxidant activity compared to crude seaweed extracts [15,21]. A high antioxidant capacity in sulfated polysaccharides has been related to a combined contribution of sulfate and phenolic content [72], where higher values are typically associated with the combined contribution of these components. In contrast, our study evaluates a purified polysaccharide fraction, in which antioxidant activity is primarily associated with sulfate groups rather than phenolic compounds.

The high sulfate content of the present polysaccharide (28%) may contribute to its antioxidant performance. Sulfate groups introduce strong negative charges along the galactan backbone, which can promote electron donation and stabilization of radical species in aqueous systems [73]. Similar structure–activity relationships have been described for sulfated galactans and agarans from red seaweeds, where increasing sulfation degree is associated with enhanced $ABTS^+$ and, to a lesser extent, DPPH radical scavenging capacities [64,74]. Notably, the antioxidant activity observed here is consistent with values reported for highly sulfated polysaccharides (typically 9–13% sulfate), highlighting the functional relevance of the unusually high sulfation level [75,76].

Previous studies on red seaweed polysaccharides provide further insight into the structure–activity relationship governing antioxidant behavior [77]. In particular, fraction-

ated polysaccharides from *Mastocarpus stellatus* showed that $ABTS^+$ radical scavenging activity varies significantly among fractions depending on their chemical composition and extraction conditions, and that sulfate content is strongly correlated with antioxidant capacity ($p < 0.001$), indicating that sulfation plays a central role in radical scavenging activity. In contrast, the influence of molecular weight was less consistent, suggesting that chemical functionality rather than chain size is the dominant factor controlling antioxidant performance.

The lower DPPH• scavenging activity relative to $ABTS^+$ can be rationalized by steric and solubility limitations inherent to the DPPH assay, which favors low-molecular-weight and more hydrophobic antioxidants [78]. Similar trends have been reported for sulfated polysaccharides from red seaweeds and marine microalgae, where high sulfate density enhances $ABTS^{\bullet+}$ scavenging but only moderately improves DPPH• reduction [16]. Taken together, these results position the present sulfated polysaccharide as a hydrophilic antioxidant, within the range reported for many red algal polysaccharides, supporting its potential application as a natural antioxidant in functional foods, nutraceuticals, and cosmetic formulations.

To further evaluate the antioxidant behavior of the sulfated polysaccharide, dose–response curves were constructed for both $ABTS^+$ and DPPH• assays (Figure 10). A concentration-dependent increase in radical scavenging activity was observed in both systems. In the $ABTS^+$ assay, the polysaccharide exhibited a progressive increase in inhibition, reaching approximately 70% at 50 mg/mL, with an estimated IC_{50} value of 31.8 ± 2.5 mg/mL. In contrast, the DPPH• assay showed lower radical-scavenging efficiency, reaching 67% inhibition at 100 mg/mL and an IC_{50} of approximately 51.1 ± 3.0 mg/mL. Statistical differences between concentrations were evaluated using one-way ANOVA ($p < 0.05$). The percentage inhibition values and statistical grouping of both $ABTS^+$ and DPPH• assays are summarized in Table 6.

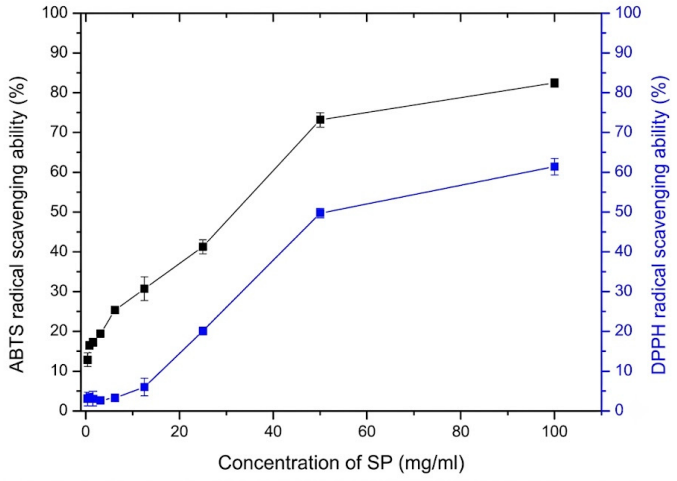

Figure 10. Dose–response curves of $ABTS^+$ and DPPH• radical scavenging activity of the sulfated polysaccharide. Data are expressed as mean ± standard deviation ($n = 6$).

The IC_{50} value observed in the $ABTS^+$ assay indicates a higher sensitivity of this method toward the sulfated polysaccharide. This behavior is consistent with the predominance of electron transfer mechanisms and the hydrophilic nature of the polymer. In contrast, the DPPH• assay, which is more suitable for low-molecular-weight and hydrophobic antioxidants, shows reduced sensitivity toward macromolecular and highly charged systems [79,80]. Polysaccharides from *Gracilaria* species have shown DPPH• IC_{50} values in the range 10–100 of mg/mL depending on sulfation degree and molecular weight [39,81], while fractionated galactans from *Mastocarpus stellatus* exhibit moderate antioxidant re-

sponses strongly correlated with sulfate content [77]. More generally, marine SPs are consistently described as exhibiting moderate IC_{50} values compared with phenolic-rich extracts, with activity largely governed by degree of sulfation and macromolecular structure [75,82]. Taken together, these results suggest that the antioxidant activity of the present sulfated polysaccharide lies within the expected range for structurally similar systems and is primarily governed by its degree of sulfation and hydrophilicity.

Table 6. Percentage inhibition (%) of $ABTS^+$ and DPPH• radical scavenging activity of the sulfated polysaccharide at different concentrations.

Concentration (mg/mL)	ABTS (% Inhibition)	DPPH (% Inhibition)
100	82.45 ± 1.10 ^{a}	61.41 ± 2.13 ^{a}
50	70.23 ± 1.85 ^{b}	49.74 ± 1.15 ^{b}
25	37.31 ± 1.77 ^{c}	20.11 ± 0.64 ^{c}
12.5	30.75 ± 2.96 ^{d}	6.00 ± 2.15 ^{d}
6.25	25.34 ± 0.82 ^{d}	3.29 ± 0.98 ^{e}
3.125	19.45 ± 0.60 ^{e}	2.66 ± 0.39 ^{e}
1.5625	17.21 ± 1.01 ^{e}	3.10 ± 1.86 ^{e}
0.78125	16.53 ± 0.97 ^{e}	3.56 ± 0.14 ^{e}
0.390625	12.88 ± 1.66 ^{e}	3.06 ± 1.72 ^{e}

Values are expressed as mean ± standard deviation (n = 6). Different superscript letters within each column indicate significant differences ($p < 0.05$) according to one-way ANOVA followed by Tukey–Kramer test.

3.7. Fe^{3+}-Induced Complexation and Microgel Formation of the Sulfated Polysaccharide

The interaction between the sulfated polysaccharide and trivalent iron ions (Fe^{3+}) was evaluated at a polymer concentration of 2% (w/v), revealing a strong affinity between the polymer chains and the metal ions. Upon mixing with Fe^{3+}, an immediate macroscopic precipitation was observed, accompanied by the formation of heterogeneous microgel-like aggregates, as shown in Figure 11. Optical microscopy images showed irregularly shaped, dense microstructures consistent with ion-induced aggregation and polysaccharide association. These observations suggest that Fe^{3+} can promote intermolecular association between sulfated polysaccharide chains.

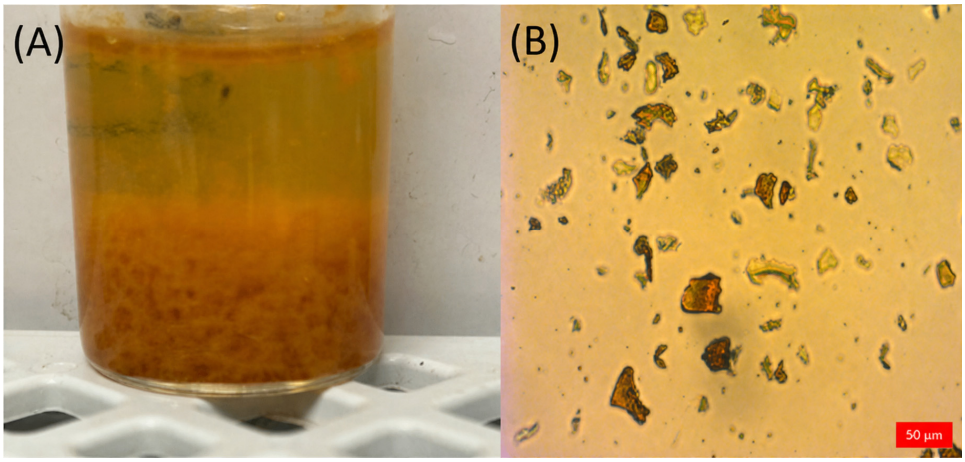

Figure 11. (**A**) Macroscopic appearance and (**B**) optical microscopy image at 40× magnification of the microgel-like aggregates formed upon addition of Fe^{3+} to the sulfated polysaccharide solution. Scale bar = 50 µm.

Electrostatic interactions between Fe^{3+} ions and negatively charged groups along the polysaccharide backbone are likely involved in the formation of the observed microgel-like

aggregates. Fe^{3+} can bridge neighboring chains due to the polymer's high sulfate concentration, thereby promoting intermolecular interactions and network development via ionic crosslinking. For highly sulfated galactans like carrageenans, similar ion-mediated gelation or precipitation conditions have been observed. Multivalent cations cause chain aggregation by neutralizing sulfate charges, generating interface zones [2,23]. Yao, et al. [83] demonstrate for the first time that λ-carrageenan, a highly sulfated polysaccharide (3 sulfates/disaccharide) from red seaweed *Gigartina lanceata*, forms thermally stable gels with Fe^{3+} ions, expanding its utility beyond a viscosifier. Moreover, Fe^{3+} addition (0.4% $FeCl_3$ to 1% PS) instantly precipitates a fibrous gel, unlike Na^+/Ca^{2+} forms that remain viscous; rheology shows G′ (1200 Pa) >> G″ (150 Pa) at 5 °C, stable to 70 °C without crossover, and frequency-independent elasticity (0.1–100 Hz) [23]. ImageJ analysis of three representative optical micrographs, including approximately 60 measured structures, revealed a broad and heterogeneous apparent size distribution. Particle size was expressed as the equivalent circular diameter. Most of the Fe^{3+}-induced structures were observed within the 5–20 μm range, while some irregular aggregates exceeded 50 μm. These findings are consistent with the formation of polydisperse microgel-like aggregates rather than a uniform particle population.

This behavior is particularly relevant because it indicates the sulfated polysaccharides' strong ion-responsive character. Trivalent ions such as Fe^{3+} can act as efficient ionic crosslinkers by bridging negatively charged sulfate groups located on different polysaccharide chains. This mechanism is consistent with previous reports on λ-carrageenan, where Fe^{3+} was shown to induce gelation in a highly sulfated polysaccharide system that otherwise behaves mainly as a viscous solution depending on the source and type of polysaccharide [84,85]. Similar observations have been discussed for algal polysaccharide hydrogels, where trivalent cations such as Fe^{3+} and Al^{3+} interact specifically with highly charged polysaccharide chains and promote network formation [86]. This ion-responsive behavior may justify further investigation of the polysaccharide as a precursor for ion-crosslinked hydrocolloid or biomaterial systems. The relevance of sulfated polysaccharides in hydrogel and biomedical material design has been highlighted in recent reviews, where sulfate groups are described as functional motifs capable of modulating ion interactions, transient crosslinking, swelling, and bioactivity [37].

FTIR spectroscopy further supported the Fe^{3+}-mediated polysaccharide association of polysaccharide–Fe^{3+} interactions (Figure 12). The spectrum of the native sulfated polysaccharide showed a broad O–H stretching band centered around 3500 cm^{-1}, as well as characteristic sulfate ester vibrations near 1214 cm^{-1}, assigned to asymmetric S=O stretching, and bands around 930 and 845 cm^{-1}, commonly associated with galactan structures and sulfate substitution patterns. After complexation with Fe^{3+}, noticeable changes in band intensity and shape were observed, particularly a reduction and broadening of the O–H stretching band and modifications in sulfate-related absorptions. These changes suggest interactions between Fe^{3+} ions and oxygen-containing functional groups of the polysaccharide, mainly hydroxyl and sulfate ester groups. Similar spectral changes have been reported for Fe^{3+}–sulfated polysaccharide complexes, where Fe^{3+} coordination affects the O–H region and sulfate-associated bands while preserving the main carbohydrate backbone vibrations, including the region around 930 cm^{-1} [87].

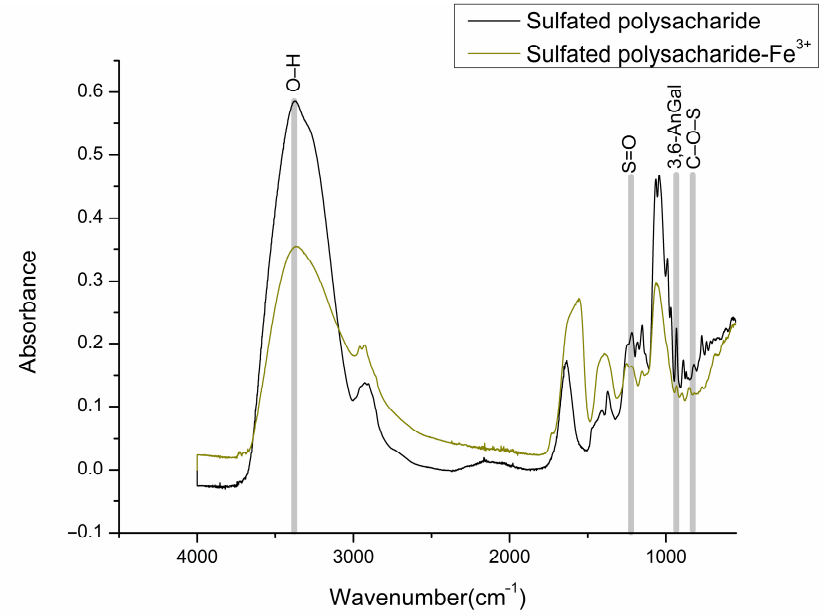

Figure 12. FTIR spectra of the sulfated polysaccharide before and after complexation with Fe^{3+}.

The Fe^{3+}-induced association observed in the sulfated polysaccharide suggests its potential as an ion-responsive hydrocolloid. However, further studies on microgel size distribution, stability, mechanical properties, and ion-binding mechanisms are required to confirm its applicability as a functional biomaterial. For example, Fe^{3+}-crosslinked alginate networks have been explored as structured biomaterials for controlled-release systems, injectable hydrogels, and bioactive carriers due to coordination between trivalent iron ions and anionic functional groups in the polymer backbone [54].

Overall, the combined macroscopic, microscopic, and spectroscopic evidence is consistent with Fe^{3+}-mediated ionic association and the formation of heterogeneous microgel-like aggregates. However, the exact coordination environment of Fe^{3+} and the relative contributions of sulfate and hydroxyl groups require further confirmation by complementary techniques. The Fe^{3+}-induced association observed in the sulfated polysaccharide suggests potential relevance for the development of ion-responsive hydrocolloid systems. Nevertheless, the present results should be considered preliminary, and further studies on particle stability, rheological behavior, iron-binding capacity, release kinetics, cytocompatibility, and performance under application-relevant conditions are required before specific food, nutraceutical, or biomedical applications can be proposed.

4. Conclusions

This study shows that the analyzed *G. vermiculophylla* specimen is a valuable source of sulfated galactan, whose functional behavior is mainly influenced by sulfate density, substitution pattern, and chain conformation. The polysaccharide has high carbohydrate (97%) and sulfate (28%) contents, making it more highly sulfated than many reported agarans from red macroalgae. Spectroscopic analyses supported an agaran-type sulfated galactan with 3,6-anhydrogalactose-type residues and sulfate-associated environments possibly related to C-6 positions, leading to expanded chain conformations and a large hydrodynamic volume, as indicated by a high intrinsic viscosity (420.9 mL/g) despite a moderate molecular weight (Mw = 2.39 × 10^5 g/mol). These traits allow the formation of weak yet stable physical gels at 3% *w*/*v* and enhance responsiveness to multivalent cations, particularly Fe^{3+} ions. From a functional perspective, the elevated sulfate density correlates with antioxidant activity, particularly in aqueous systems ($ABTS^+$ = 172.4 ± 6.8 µmol TE/g; IC_{50} = 31.8 ± 2.5 mg/mL),

while DPPH• showed lower activity (51.1 ± 3.0 μmol TE/g; IC_{50} = 51.1 ± 3.0 mg/mL). In addition, pronounced complexation with Fe^{3+} enabled rapid ion-mediated aggregation and microgel formation. Overall, these findings highlight the potential of the *Gracilaria*-derived sulfated galactan characterized in this study as a responsive and bioactive marine biopolymer. Future work should explore how ionic strength, cation type, pH, and complex matrices influence its gelation behavior, microstructure, and functional performance.

Author Contributions: Conceptualization, D.E.-B. and E.C.-M.; methodology, D.E.-B., E.C.-M., J.M.-E. and K.G.M.-R.; validation, D.E.-B., E.C.-M., J.M.-E., K.G.M.-R. and A.C.C.-M.; formal analysis, D.E.-B., E.C.-M., R.P.-G., J.M.-E. and K.G.M.-R.; investigation, D.E.-B., E.C.-M., J.M.-E., K.G.M.-R. and A.C.C.-M.; data curation, D.E.-B., E.C.-M., J.M.-E. and K.G.M.-R.; writing—original draft preparation, D.E.-B., E.C.-M. and A.C.C.-M.; writing—review and editing, D.E.-B., E.C.-M., J.M.-E., R.P.-G., K.G.M.-R. and A.C.C.-M.; visualization, D.E.-B. and E.C.-M.; supervision, E.C.-M.; project administration, E.C.-M. All authors have read and agreed to the published version of the manuscript.

Funding: This research was supported by Secretaría de Ciencia, Humanidades, Tecnología e Innovación (SECIHTI) (Project No. 319684).

Data Availability Statement: The original contributions presented in this study are included in the article. Further inquiries can be directed to the corresponding authors.

Acknowledgments: The authors acknowledge for the postdoctoral fellowship awarded to David Encinas-Basurto.

Conflicts of Interest: The authors declare no competing interests.

Abbreviations

The following abbreviations are used in this manuscript:

ABTS	2,2′-Azino-bis(3-ethylbenzothiazoline-6-sulfonic acid) radical cation
DPPH	2,2-Diphenyl-1-picrylhydrazyl radical
FTIR	Fourier transform infrared spectroscopy
GC	Gas chromatography
G′	Storage modulus
G″	Loss modulus
MALS	Multi-angle laser light scattering
Mn	Number-average molar mass
Mw	Weight-average molar mass
NMR	Nuclear magnetic resonance
SP	Polysaccharide
Rh	Hydrodynamic radius
Rg	Radius of gyration
RI	Refractive index
SEC	Size-exclusion chromatography
TE	Trolox equivalent antioxidant capacity
[η]	Intrinsic viscosity

References

1. Encinas-Basurto, D.; Marquez-Escalante, J.; Miranda-Baeza, A.; Carvajal-Millán, E. Innovative applications of sulfated polysaccharides from macroalgae in hydrogels and biomaterials production. *AIMS Bioeng.* **2025**, *12*, 556–592. [CrossRef]
2. Elmarhoum, S.; Mathieu, S.; Ako, K.; Helbert, W. Sulfate groups position determines the ionic selectivity and syneresis properties of carrageenan systems. *Carbohydr. Polym.* **2023**, *299*, 120166. [CrossRef] [PubMed]
3. Matsuhiro, B.; Barahona, T.; Encinas, M.V.; Mansilla, A.; Ortiz, J.A. Sulfation of agarose from subantarctic *Ahnfeltia plicata* (Ahnfeltiales, Rhodophyta): Studies of its antioxidant and anticoagulant properties in vitro and its copolymerization with acrylamide. *J. Appl. Phycol.* **2014**, *26*, 2011–2019. [CrossRef]

4. Li, J.; Ye, G.; Wang, J.; Gong, T.; Wang, J.; Zeng, D.; Cifuentes, A.; Ibañez, E.; Zhao, H.; Lu, W. Recent advances in pressurized hot water extraction/modification of polysaccharides: Structure, physicochemical properties, bioactivities, and applications. *Compr. Rev. Food Sci. Food Saf.* **2025**, *24*, e70104. [CrossRef] [PubMed]
5. Hentati, F.; Delattre, C.; Gardarin, C.; Desbrières, J.; Le Cerf, D.; Rihouey, C.; Michaud, P.; Abdelkafi, S.; Pierre, G. Structural features and rheological properties of a sulfated Xylogalactan-rich fraction isolated from Tunisian red seaweed *Jania adhaerens*. *Appl. Sci.* **2020**, *10*, 1655. [CrossRef]
6. Halperin-Sternfeld, M.; Netanel Liberman, G.; Kannan, R.; Netti, F.; Ma, P.X.; Arad, S.M.; Adler-Abramovich, L. Thixotropic red microalgae sulfated polysaccharide-peptide composite hydrogels as scaffolds for tissue engineering. *Biomedicines* **2022**, *10*, 1388. [CrossRef] [PubMed]
7. Fanina, S.; Casillo, A.; Corsaro, M.M. Mediterranean Seaweed Polysaccharides: Insight into Chemical Structures, Applications, and Structure/Application Correlations. *Mar. Drugs* **2025**, *24*, 11. [CrossRef] [PubMed]
8. Anaya-Rosas, R.E.; Rivas-Vega, M.E.; Miranda-Baeza, A.; Piña-Valdez, P.; Nieves-Soto, M. Effects of a co-culture of marine algae and shrimp (*Litopenaeus vannamei*) on the growth, survival and immune response of shrimp infected with *Vibrio parahaemolyticus* and white spot virus (WSSV). *Fish Shellfish Immunol.* **2019**, *87*, 136–143. [CrossRef] [PubMed]
9. Anaya-Rosas, R.E.; Nieves-Soto, M.; Rivas-Vega, M.E.; Miranda-Baeza, A.; Piña-Valdez, P. Antioxidant activity and apparent digestibility of amino acids of three macroalgae meals in the diets of Pacific white shrimp (*Litopenaeus vannamei*). *Lat. Am. J. Aquat. Res.* **2017**, *45*, 970–978. [CrossRef]
10. Sánchez-Romero, A.; Miranda-Baeza, A.; López-Elías, J.A.; Martínez-Córdova, L.R.; Tejeda-Mansir, A.; Márquez-Ríos, E. Effect of the photoperiod and the shrimp-macroalgae rate on removal of total ammonia nitrogen by *Gracilaria vermiculophylla*, cultivated with *Litopenaeus vannamei*, without water exchange. *Lat. Am. J. Aquat. Res.* **2013**, *41*, 888–897.
11. da Silva Chagas, F.D.; Lima, G.C.; Dos Santos, V.I.N.; Costa, L.E.C.; de Sousa, W.M.; Sombra, V.G.; de Araújo, D.F.; Barros, F.C.N.; Marinho-Soriano, E.; de Andrade Feitosa, J.P. Sulfated polysaccharide from the red algae *Gelidiella acerosa*: Anticoagulant, antiplatelet and antithrombotic effects. *Int. J. Biol. Macromol.* **2020**, *159*, 415–421. [CrossRef]
12. DuBois, M.; Gilles, K.A.; Hamilton, J.K.; Rebers, P.A.; Smith, F. Colorimetric method for determination of sugars and related substances. *Anal. Chem.* **1956**, *28*, 350–356. [CrossRef]
13. Terho, T.T.; Hartiala, K. Method for determination of the sulfate content of glycosaminoglycans. *Anal. Biochem.* **1971**, *41*, 471–476. [CrossRef] [PubMed]
14. Rouau, X.; Surget, A. A rapid semi-automated method for the determination of total and water-extractable pentosans in wheat flours. *Carbohydr. Polym.* **1994**, *24*, 123–132. [CrossRef]
15. Fimbres-Olivarria, D.; Marquez-Escalante, J.; Martínez-Robinson, K.G.; Miranda-Arizmendi, V.; Anda-Flores, Y.D.; Rascon-Chu, A.; Brown-Bojorquez, F.; Carvajal-Millan, E. Physicochemical and microstructural characteristics of sulfated polysaccharide from marine microalga. *Analytica* **2023**, *4*, 527–537. [CrossRef]
16. Miranda-Arizmendi, V.; Fimbres-Olivarria, D.; Miranda-Baeza, A.; Martínez-Robinson, K.; Rascón-Chu, A.; De Anda-Flores, Y.; Lizardi-Mendoza, J.; Mendez-Encinas, M.A.; Brown-Bojorquez, F.; Canett-Romero, R. Sulfated polysaccharides from Chaetoceros muelleri: Macromolecular characteristics and bioactive properties. *Biology* **2022**, *11*, 1476. [CrossRef] [PubMed]
17. Cruz-Amaya, K.S.; Hernández-Martínez, D.; Del-Toro-Sánchez, C.L.; Carvajal-Millan, E.; Martínez-Robinson, K.; DeAnda-Flores, Y.B.; Cornejo-Ramírez, Y.I. Synthesis and characterization of triticale starch-based hydrogel for pH responsive controlled diffusion. *ACS Omega* **2024**, *9*, 28564–28576. [CrossRef] [PubMed]
18. Bernal-Mercado, A.T.; Vazquez-Armenta, F.J.; Tapia-Rodriguez, M.R.; Islas-Osuna, M.A.; Mata-Haro, V.; Gonzalez-Aguilar, G.A.; Lopez-Zavala, A.A.; Ayala-Zavala, J.F. Comparison of single and combined use of catechin, protocatechuic, and vanillic acids as antioxidant and antibacterial agents against uropathogenic *Escherichia coli* at planktonic and biofilm levels. *Molecules* **2018**, *23*, 2813. [CrossRef] [PubMed]
19. Martínez-López, A.; Carvajal-Millan, E.; López-Franco, Y.; Lizardi-Mendoza, J.; Rascón-Chu, A. Antioxidant activity of maize bran arabinoxylan microspheres. In *Food Composition and Analysis: Methods and Strategies*; Taylor & Francis Group: Abingdon, UK, 2014; pp. 19–28.
20. Marquez-Escalante, J.A.; Carvajal-Millan, E. Feruloylated arabinoxylans from Maize Distiller's dried grains with solubles: Effect of feruloyl esterase on their macromolecular characteristics, gelling, and antioxidant properties. *Sustainability* **2019**, *11*, 6449. [CrossRef]
21. González-Vega, R.I.; Del-Toro-Sánchez, C.L.; Moreno-Corral, R.A.; López-Elías, J.A.; Reyes-Díaz, A.; García-Lagunas, N.; Carvajal-Millán, E.; Fimbres-Olivarría, D. Sulfated polysaccharide-rich extract from *Navicula incerta*: Physicochemical characteristics, antioxidant activity, and anti-hemolytic property. *AIMS Bioeng.* **2022**, *9*, 364–382. [CrossRef]
22. Fimbres-Olivarria, D.; Carvajal-Millan, E.; Lopez-Elias, J.A.; Martinez-Robinson, K.G.; Miranda-Baeza, A.; Martinez-Cordova, L.R.; Enriquez-Ocaña, F.; Valdez-Holguin, J.E. Chemical characterization and antioxidant activity of sulfated polysaccharides from *Navicula* sp. *Food Hydrocoll.* **2018**, *75*, 229–236. [CrossRef]

23. Fimbres-Olivarría, D.; López-Elías, J.A.; Carvajal-Millán, E.; Márquez-Escalante, J.A.; Martínez-Córdova, L.R.; Miranda-Baeza, A.; Enríquez-Ocaña, F.; Valdéz-Holguín, J.E.; Brown-Bojórquez, F. Navicula sp. sulfated polysaccharide gels induced by Fe (III): Rheology and microstructure. *Int. J. Mol. Sci.* **2016**, *17*, 1238. [CrossRef] [PubMed]
24. Campo, V.L.; Kawano, D.F.; Silva, D.B.d.; Carvalho, I. Carrageenans: Biological properties, chemical modifications and structural analysis—A review. *Carbohydr. Polym.* **2009**, *77*, 167–180. [CrossRef]
25. Premarathna, A.D.; Ahmed, T.A.; Kulshreshtha, G.; Humayun, S.; Darko, C.N.S.; Rjabovs, V.; Hammami, R.; Critchley, A.T.; Tuvikene, R.; Hincke, M.T. Polysaccharides from red seaweeds: Effect of extraction methods on physicochemical characteristics and antioxidant activities. *Food Hydrocoll.* **2024**, *147*, 109307. [CrossRef]
26. Hentati, F.; Tounsi, L.; Pierre, G.; Barkallah, M.; Ursu, A.V.; Ben Hlima, H.; Desbrières, J.; Le Cerf, D.; Fendri, I.; Michaud, P. Structural characterization and rheological and antioxidant properties of novel polysaccharide from calcareous red seaweed. *Mar. Drugs* **2022**, *20*, 546. [CrossRef] [PubMed]
27. Figueroa, F.A.; Abdala-Díaz, R.T.; Pérez, C.; Casas-Arrojo, V.; Nesic, A.; Tapia, C.; Durán, C.; Valdes, O.; Parra, C.; Bravo-Arrepol, G. Sulfated polysaccharide extracted from the green algae *Codium bernabei*: Physicochemical characterization and antioxidant, anticoagulant and antitumor activity. *Mar. Drugs* **2022**, *20*, 458. [CrossRef] [PubMed]
28. Ciancia, M.; Matulewicz, M.C.; Tuvikene, R. Structural diversity in galactans from red seaweeds and its influence on rheological properties. *Front. Plant Sci.* **2020**, *11*, 559986. [CrossRef] [PubMed]
29. Sánchez, R.A.R.; Canelón, D.J.; Cosenza, V.A.; Fissore, E.N.; Gerschenson, L.N.; Matulewicz, M.C.; Ciancia, M. Gracilariopsis hommersandii, a red seaweed, source of agar and sulfated polysaccharides with unusual structures. *Carbohydr. Polym.* **2019**, *213*, 138–146. [CrossRef]
30. Manuhara, G.J.; Praseptiangga, D.; Riyanto, R.A. Extraction and characterization of refined K-carrageenan of red algae [*Kappaphycus Alvarezii* (Doty ex PC Silva, 1996)] originated from Karimun Jawa Islands. *Aquat. Procedia* **2016**, *7*, 106–111. [CrossRef]
31. Diharmi, A.; Irasari, N. Characteristic of carrageenan *Eucheuma cottonii* collected from the coast of Tanjung Medang Village and Jaga Island, Riau. In *IOP Conference Series: Earth and Environmental Science, Volume 404, Proceedings of the 4th EMBRIO International Symposium and the 7th International Symposium of East Asia Fisheries and Technologists Association, Bogor, Indonesia, 5–6 August 2019*; IOP Publishing: Bristol, UK, 2019; p. 012049.
32. Lahaye, M.; Rochas, C. Chemical structure and physico-chemical properties of agar. *Hydrobiologia* **1991**, *221*, 137–148. [CrossRef]
33. Darko, C.N.S.; Arthur, B.; Saluri, K.; Lepik, H.; Punak, L.; Robal, M.; Martma, K.; Tuvikene, R. Influence of alkali treatment and ultrasonication on the bioactivities and rheological properties of sulfated polysaccharides. *Int. J. Biol. Macromol.* **2025**, *314*, 144122. [CrossRef] [PubMed]
34. Gopu, M.; Selvam, K. Polysaccharides from marine red algae *Amphiroa rigida* and their biomedical potential: An in-vitro study. *Biocatal. Agric. Biotechnol.* **2020**, *29*, 101769. [CrossRef]
35. Liu, Y.; Liu, W.; Wang, Y.; Ma, Y.; Huang, L.; Zou, C.; Li, D.; Cao, M.-J.; Liu, G.-M.J.M.d. Inhibitory effect of depolymerized sulfated galactans from marine red algae on the growth and adhesion of diarrheagenic *Escherichia coli*. *Mar. Drugs* **2019**, *17*, 694. [CrossRef] [PubMed]
36. Makshakova, O.; Faizullin, D.; Zuev, Y.F. Interplay between secondary structure and ion binding upon thermoreversible gelation of κ-carrageenan. *Carbohydr. Polym.* **2020**, *227*, 115342. [CrossRef] [PubMed]
37. Arlov, Ø.; Rütsche, D.; Asadi Korayem, M.; Öztürk, E.; Zenobi-Wong, M. Engineered sulfated polysaccharides for biomedical applications. *Adv. Funct. Mater.* **2021**, *31*, 2010732. [CrossRef]
38. Kazachenko, A.S.; Vasilieva, N.Y.; Malyar, Y.N.; Karacharov, A.A.; Kondrasenko, A.A.; Levdanskiy, A.V.; Borovkova, V.S.; Miroshnikova, A.V.; Issaoui, N.; Kazachenko, A.S. Sulfation of arabinogalactan with ammonium sulfamate. *Biomass Convers. Biorefinery* **2024**, *14*, 719–731.
39. Khan, B.M.; Qiu, H.-M.; Wang, X.-F.; Liu, Z.-Y.; Zhang, J.-Y.; Guo, Y.-J.; Chen, W.-Z.; Liu, Y.; Cheong, K.-L. Physicochemical characterization of *Gracilaria chouae* sulfated polysaccharides and their antioxidant potential. *Int. J. Biol. Macromol.* **2019**, *134*, 255–261. [CrossRef] [PubMed]
40. Genicot-Joncour, S.; Poinas, A.; Richard, O.; Potin, P.; Rudolph, B.; Kloareg, B.; Helbert, W. The cyclization of the 3, 6-anhydrogalactose ring of ι-carrageenan is catalyzed by two D-galactose-2, 6-sulfurylases in the red alga *Chondrus crispus*. *Plant Physiol.* **2009**, *151*, 1609–1616. [CrossRef] [PubMed]
41. Zamanileha, E.F.; Mitantsoa, J.T.; Vaonalamihanta, P.F.; Razafintsalama, A.R.; Andrianony, F.A.; Hervé, R.P. Various Approaches to Fourier-Transform Infrared Spectroscopy (FTIR) for Bioanalytical and Biotechnological Applications in Marine Algae. In *Recent Advances in Infrared Spectroscopy and Its Applications in Biotechnology*; IntechOpen: London, UK, 2024.
42. Pereira, L.; Amado, A.M.; Critchley, A.T.; van de Velde, F.; Ribeiro-Claro, P.J.A. Identification of selected seaweed polysaccharides (phycocolloids) by vibrational spectroscopy (FTIR-ATR and FT-Raman). *Food Hydrocoll.* **2009**, *23*, 1903–1909. [CrossRef]
43. Gieroba, B.; Kalisz, G.; Krysa, M.; Khalavka, M.; Przekora, A. Application of vibrational spectroscopic techniques in the study of the natural polysaccharides and their cross-linking process. *Int. J. Mol. Sci.* **2023**, *24*, 2630. [CrossRef] [PubMed]

44. Jiang, Z.; Yu, G.; Liang, Y.; Song, T.; Zhu, Y.; Ni, H.; Yamaguchi, K.; Oda, T. Inhibitory effects of a sulfated polysaccharide isolated from edible red alga *Bangia fusco*-purpurea on α-amylase and α-glucosidase. *Biosci. Biotechnol. Biochem.* **2019**, *83*, 2065–2074. [CrossRef] [PubMed]
45. Li, X.; Yao, W.; Hu, C.; Lin, C.; You, L.; Mao, J. Comparative Analysis of *Gracilaria chouae* Polysaccharides Derived from Different Geographical Regions: Focusing on Their Chemical Composition, Rheological Properties, and Gel Characteristics. *Gels* **2024**, *10*, 454. [CrossRef] [PubMed]
46. Atya, M.E.; Tuvikene, R.; Matsukawa, S. Kinetic behavior of the network structure changes in funoran gelation studied by rheological and NMR measurements. *Carbohydr. Polym. Technol. Appl.* **2024**, *7*, 100415. [CrossRef]
47. Korva, H.; Kärkkäinen, J.; Lappalainen, K.; Lajunen, M. Spectroscopic study of natural and synthetic polysaccharide sulfate structures. *Starch-Stärke* **2016**, *68*, 854–863. [CrossRef]
48. Darko, C.N.S.; Humayun, S.; Premarathna, A.D.; Howlader, M.M.; Rjabovs, V.; Tuvikene, R. Rheology and characterization of sulfated agarans from the edible epiphytic red alga, *Vertebrata lanosa* (truffle seaweed). *Food Hydrocoll.* **2024**, *151*, 109770. [CrossRef]
49. Fernando, I.S.; Sanjeewa, K.A.; Samarakoon, K.W.; Lee, W.W.; Kim, H.-S.; Kim, E.-A.; Gunasekara, U.; Abeytunga, D.; Nanayakkara, C.; De Silva, E. FTIR characterization and antioxidant activity of water soluble crude polysaccharides of Sri Lankan marine algae. *Algae* **2017**, *32*, 75. [CrossRef]
50. Atya, M.E.; Yang, X.; Tashiro, Y.; Tuvikene, R.; Matsukawa, S. Structural and physicochemical characterization of funoran extracted from *Gloiopeltis furcata* by different methods. *Algal Res.* **2023**, *76*, 103334. [CrossRef]
51. Gong, G.; Zhao, J.; Wang, C.; Wei, M.; Dang, T.; Deng, Y.; Sun, J.; Song, S.; Huang, L.; Wang, Z. Structural characterization and antioxidant activities of the degradation products from *Porphyra haitanensis* polysaccharides. *Process Biochem.* **2018**, *74*, 185–193. [CrossRef]
52. Fontana, C.; Widmalm, G. Primary structure of glycans by NMR spectroscopy. *Chem. Rev.* **2023**, *123*, 1040–1102. [CrossRef] [PubMed]
53. Rudtanatip, T.; Somintara, S.; Sakaew, W.; El-Abid, J.; Cano, M.E.; Jongsomchai, K.; Wongprasert, K.; Kovensky, J. Sulfated galactans from *Gracilaria fisheri* with supplementation of octanoyl promote wound healing activity in vitro and in vivo. *Macromol. Biosci.* **2022**, *22*, 2200172. [CrossRef]
54. Liu, H.; Chen, X.; Chen, D.; Zhang, Z.; Xia, Y.; Zhang, K.; Ming, J.; Lei, X. Decoding the molecular interaction mechanisms of tannic acid in modulating Fe3+-sodium alginate microgel delivery systems. *Food Chem.* **2025**, *489*, 144935. [CrossRef] [PubMed]
55. Castro, J.P.L.d.; Costa, L.E.C.; Pinheiro, M.P.; Francisco, T.d.S.; Vasconcelos, P.H.M.d.; Funari, L.M.; Daudt, R.M.; Santos, G.R.C.d.; Cardozo, N.S.M.; Freitas, A.L.P. Polysaccharides of red alga *Gracilaria intermedia*: Structure, antioxidant activity and rheological behavior. *Polímeros* **2018**, *28*, 178–186. [CrossRef]
56. Liu, P.; Li, F.; Liu, Z.; Liu, Y. Novel Sulfated Oligosaccharide DP9 from Marine Algae, *Gracilaria lemaneiformis*: A Potent Galectin-3 Inhibitor for Pancreatic Cancer Therapy. *Mar. Drugs* **2025**, *23*, 423. [CrossRef] [PubMed]
57. Soares, P.A.; Queiroz, I.N.; Pomin, V.H. NMR structural biology of sulfated glycans. *J. Biomol. Struct. Dyn.* **2017**, *35*, 1069–1084. [PubMed]
58. Costa, L.E.C.; Brito, T.V.; Damasceno, R.O.S.; Sousa, W.M.; Barros, F.C.N.; Sombra, V.G.; Júnior, J.S.C.; Magalhães, D.A.; Souza, M.H.; Medeiros, J.-V.R. Chemical structure, anti-inflammatory and antinociceptive activities of a sulfated polysaccharide from *Gracilaria intermedia* algae. *Int. J. Biol. Macromol.* **2020**, *159*, 966–975. [CrossRef] [PubMed]
59. Sanchez, R.A.R.; Saluri, K.; Tuvikene, R.; Matulewicz, M.C.; Ciancia, M. Complex sulfated galactans from hot water extracts of red seaweed *Asparagopsis taxiformis* comprise carrageenan and agaran structures. *Carbohydr. Polym.* **2023**, *322*, 121314. [CrossRef]
60. Rubinstein, M.; Colby, R.H. *Polymer Physics*; Oxford University Press: Oxford, UK, 2003.
61. Mezger, T. *The Rheology Handbook: For Users of Rotational and Oscillatory Rheometers*; Vincentz Network GmbH & Co. KG: Hanover, Germany, 2020.
62. Lee, Y.; Bak, J. Rheological Properties of Fucoidan–Xanthan Gum Mixture in the Presence of Simulated Salivary Fluid and Its Anti-Inflammatory Effect after In Vitro Digestion. *Biomacromolecules* **2025**, *26*, 3795–3804. [CrossRef] [PubMed]
63. Haydukivska, K.; Blavatska, V.; Paturej, J. Universal size ratios of Gaussian polymers with complex architecture: Radius of gyration vs hydrodynamic radius. *Sci. Rep.* **2020**, *10*, 14127. [CrossRef] [PubMed]
64. Khan, B.M.; Zheng, L.-X.; Khan, W.; Shah, A.A.; Liu, Y.; Cheong, K.-L. Antioxidant potential of physicochemically characterized Gracilaria blodgettii sulfated polysaccharides. *Polymers* **2021**, *13*, 442. [CrossRef] [PubMed]
65. Alghooneh, A.; Razavi, S.M.; Kasapis, S. Classification of hydrocolloids based on small amplitude oscillatory shear, large amplitude oscillatory shear, and textural properties. *J. Texture Stud.* **2019**, *50*, 520–538. [CrossRef] [PubMed]
66. Kasaai, M.R. Intrinsic viscosity–molecular weight relationship and hydrodynamic volume for pullulan. *J. Appl. Polym. Sci.* **2006**, *100*, 4325–4332. [CrossRef]
67. Jumel, K. Molar mass determination of complex bioglycopolymers by size exclusion chromatography and light scattering detection. *J. Chromatogr. Libr.* **2002**, *66*, 305–345. [CrossRef]

68. Wang, F.-S.; Kosovsky, L.M.; Krist, E.C.; Kruse, B.J.; Zhukhovitskiy, A.V. Trapped entanglements in polymer networks: Formation and characterization. *Trends Chem.* **2024**, *6*, 447–458. [CrossRef]
69. Morris, V. Gelation of polysaccharides. *Funct. Prop. Food Macromol.* **1998**, *2*, 141–226.
70. Fontes-Candia, C.; Ström, A.; Lopez-Sanchez, P.; López-Rubio, A.; Martínez-Sanz, M. Rheological and structural characterization of carrageenan emulsion gels. *Algal Res.* **2020**, *47*, 101873. [CrossRef]
71. Delattre, C.; Fenoradosoa, T.A.; Michaud, P. Galactans: An overview of their most important sourcing and applications as natural polysaccharides. *Braz. Arch. Biol. Technol.* **2011**, *54*, 1075–1092. [CrossRef]
72. Torres, M.D.; Flórez-Fernández, N.; Dominguez, H. Ultrasound-assisted water extraction of mastocarpus stellatus carrageenan with adequate mechanical and antiproliferative properties. *Mar. Drugs* **2021**, *19*, 280. [CrossRef] [PubMed]
73. Li, J.; Lv, S.; Hu, Y.; Kong, Y.; Cai, J.; Nan, G.; Jiang, S.; Yang, S.; Dong, C. Regulating polysaccharide structure and bioactivity via free radical degradation: A review of mechanisms, effects, and application prospects. *Front. Nutr.* **2026**, *13*, 1725700. [CrossRef] [PubMed]
74. Aluta, U.P.; Aderolu, A.Z.; Ishola, I.O.; Alyassin, M.; Morris, G.A.; Olajide, O.A. Chemical characterisation of sulfated polysaccharides from the red seaweed *Centroceras clavulatum* and their in vitro immunostimulatory and antioxidant properties. *Food Hydrocoll. Health* **2023**, *3*, 100135. [CrossRef]
75. Rocha de Souza, M.C.; Marques, C.T.; Guerra Dore, C.M.; Ferreira da Silva, F.R.; Oliveira Rocha, H.A.; Leite, E.L. Antioxidant activities of sulfated polysaccharides from brown and red seaweeds. *J. Appl. Phycol.* **2007**, *19*, 153–160. [CrossRef] [PubMed]
76. Yu, G.; Zhang, Q.; Wang, Y.; Yang, Q.; Yu, H.; Li, H.; Chen, J.; Fu, L. Sulfated polysaccharides from red seaweed *Gelidium amansii*: Structural characteristics, anti-oxidant and anti-glycation properties, and development of bioactive films. *Food Hydrocoll.* **2021**, *119*, 106820. [CrossRef]
77. Gómez-Ordóñez, E.; Jiménez-Escrig, A.; Rupérez, P. Bioactivity of sulfated polysaccharides from the edible red seaweed *Mastocarpus stellatus*. *Bioact. Carbohydr. Diet. Fibre* **2014**, *3*, 29–40. [CrossRef]
78. Ma, X.-T.; Sun, X.-Y.; Yu, K.; Gui, B.-S.; Gui, Q.; Ouyang, J.-M. Effect of Content of Sulfate Groups in Seaweed Polysaccharides on Antioxidant Activity and Repair Effect of Subcellular Organelles in Injured HK-2 Cells. *Oxidative Med. Cell. Longev.* **2017**, *2017*, 2542950. [CrossRef]
79. Prior, R.L.; Wu, X.; Schaich, K. Standardized methods for the determination of antioxidant capacity and phenolics in foods and dietary supplements. *J. Agric. Food Chem.* **2005**, *53*, 4290–4302. [CrossRef] [PubMed]
80. Apak, R.; Gorinstein, S.; Böhm, V.; Schaich, K.M.; Özyürek, M.; Güçlü, K. Methods of measurement and evaluation of natural antioxidant capacity/activity (IUPAC Technical Report). *Pure Appl. Chem.* **2013**, *85*, 957–998. [CrossRef]
81. Souza, B.W.; Cerqueira, M.A.; Bourbon, A.I.; Pinheiro, A.C.; Martins, J.T.; Teixeira, J.A.; Coimbra, M.A.; Vicente, A.A. Chemical characterization and antioxidant activity of sulfated polysaccharide from the red seaweed *Gracilaria birdiae*. *Food Hydrocoll.* **2012**, *27*, 287–292. [CrossRef]
82. Fu, Y.; Jiao, H.; Sun, J.; Okoye, C.O.; Zhang, H.; Li, Y.; Lu, X.; Wang, Q.; Liu, J. Structure-activity relationships of bioactive polysaccharides extracted from macroalgae towards biomedical application: A review. *Carbohydr. Polym.* **2024**, *324*, 121533. [CrossRef] [PubMed]
83. Yao, X.; Yao, X.; Xu, K.; Wu, K.; Chen, X.; Liu, N.; Nishinari, K.; Phillips, G.O.; Jiang, F. Trivalent iron induced gelation in *Artemisia sphaerocephala* Krasch. polysaccharide. *Int. J. Biol. Macromol.* **2020**, *144*, 690–697. [CrossRef] [PubMed]
84. Running, C.A.; Falshaw, R.; Janaswamy, S. Trivalent iron induced gelation in lambda-carrageenan. *Carbohydr. Polym.* **2012**, *87*, 2735–2739. [CrossRef] [PubMed]
85. Cao, Y.; Li, S.; Fang, Y.; Nishinari, K.; Phillips, G.O.; Lerbret, A.; Assifaoui, A. Specific binding of trivalent metal ions to λ-carrageenan. *Int. J. Biol. Macromol.* **2018**, *109*, 350–356. [CrossRef] [PubMed]
86. Beaumont, M.; Tran, R.; Vera, G.; Niedrist, D.; Rousset, A.; Pierre, R.; Shastri, V.P.; Forget, A. Hydrogel-forming algae polysaccharides: From seaweed to biomedical applications. *Biomacromolecules* **2021**, *22*, 1027–1052. [CrossRef] [PubMed]
87. Wang, N.; Teng, H.; Zhang, X.; Zhang, J.; Li, L.; Zhang, J.; Fang, Q. Synthesis of a carrageenan–iron complex and its effect on flame retardancy and smoke suppression for waterborne epoxy. *Polymers* **2019**, *11*, 1677. [CrossRef] [PubMed]